Assisted upscaling of miscible CO_2-enhanced oil recovery floods using an artificial-neural-network-based optimisation algorithm

P. Ogbeiwi[1]*, K. D. Stephen[1]

[1]Institute of Geoenergy Engineering, Heriot-Watt University, Edinburgh, UK
*Corresponding author; email: prejohn73@gmail.com; po20@hw.ac.uk

This manuscript has been prepared for publication in **Transport in Porous Media**. Please note that the manuscript will undergo peer review and is yet to be formally accepted for publication. Subsequent versions of this manuscript may have slightly different content. Please feel free to contact the corresponding author; we welcome feedback

Abstract

The fine-scale compositional simulations required to accurately model miscible CO_2 flooding are unrealistic and highly computationally expensive, and upscaling procedures are required to approximate the behaviour of these fine-scale grids on more realistic coarse-scale models. These procedures include the pseudoisation of relative permeabilities which ensures the matching of large-scale effects such as the volumetric fluxes of the phases and the use of transport coefficients to better represent small-scale interactions such as the time-dependent flux of the components within the hydrocarbon phases (molecular diffusion). Most times, a mismatch between the phase fluxes of the integrated fine-scale and that of the coarse-scale is observed. The accuracy of the upscaling results can be improved by tuning some of the derived upscaled coarse-scale quantities such as the alpha factors, absolute permeability or the relative permeabilities endpoints. This process is generally computationally expensive and can be treated as a reservoir history matching problem. In this study, we present a framework to represent the dynamics of small-scale molecular diffusion, and macro-scale heterogeneity-induced channelling associated with miscible CO_2 displacements on upscaled coarser grid reservoir models. The approach applied was based on the pseudoisation of relative permeability and transport coefficients and was applied in two Society of Petroleum Engineers (SPE) benchmark reservoir models. Our results showed that the use of efficiently tuned transport coefficients led to better results so that the derived pseudo-relative permeability functions can be neglected. To reduce the associated computational expense, we proposed a novel methodology for upscaling miscible floods where a neural-network-based genetic-algorithm assisted upscaling procedure was applied. The optimisation algorithm was applied to reduce the error between the predictions of the upscaled models and a data-driven approximation model significantly reduced the computational expense associated with the assisted tuning procedure. In summary, the framework presented in this study adequately represented the small- and large-scale behaviour associated with the miscible displacements on upscaled coarse-scale reservoir models.

Introduction

During miscible CO_2 EOR and storage in hydrocarbon reservoirs, the performance of the process is dependent on the small-scale or local, and the field-scale or macroscopic sweep efficiencies. The local sweep efficiency is a function of the molecular diffusion and dispersion of the injected gas, which affects the level of miscibility attained by the injected

gas and the in-situ oil phase. On the field-scale, permeability heterogeneity, gravity segregation and other factors, influence the displacement efficiency of the miscible injection process (Blunt et al., 1993; Orr, 2004).

Small-scale effects such as mixing and molecular diffusion of components between the phases occur at small length that are at the core to intermediate scale. These effects can only be represented by grid cell lengths that are in the order of 10^{-2} – 10^{1} ft which is smaller than the average size of a grid block that is applied in typical field-scale reservoir simulations and are computationally expensive to use (Luo et al., 2018). Therefore, the use of coarse-scale grids as is commonly encountered in the field-scale simulations of CO_2 flooding inhibits the accurate calculation of the oil and gas components' composition at the field scale, resulting in inaccurate estimations of fluid recovery or retention (Luo et al., 2018). This is because the applied coarse-scale grid blocks do not account for the complexities associated with the small-scale molecular interactions between the injected and in-situ fluids.

The application of upscaling procedures can be used to reduce the associated computation costs while accurately approximating the behaviour of the fine-scale miscible CO_2 flooding. Here, coarse-scale models are constructed from the fine-grid models, so that the resulting coarse-scale models produce similar results of the principal petrophysical, fluid flow and pressure parameters. Several upscaling procedures for upscaling miscible compositional flows have been developed. In compositional simulations, the components are conserved and distributed in the hydrocarbon phases (Christie & Clifford, 1998). As a result, its simulations are more sensitive to grid coarsening than black-oil simulations because they inherently contain sub-grid heterogeneity, molecular diffusion and dispersion of the components in the phases. The incorrect splitting of the phases due to numerical diffusion, which causes the components to flow in the wrong phase, is also common. Pseudo functions can be applied to compensate for the numerical effects and the presence of small-scale flow phenomena such as molecular diffusion, viscous fingering, gravity tonguing, and so on (Darman et al., 2002; Rios et al., 2019). The compositional upscaling of miscible floods has received noteworthy attention by many authors.

A study by Camy & Emanuel, (1977) applied compositional upscaling by altering the phase compositions in the flow equations using factors that were calculated from one-dimensional fine-grid models. Their results showed that the use of pseudo relative permeability and *K*-values functions reduces the effects of grid coarsening in compositional simulation. Fayers et al., (1989) modified this approach using a dual-zone mixing (DZM) model which upscales compositional flows to incorporate the omission of small-scale heterogeneities in the coarse-

scale grid blocks. Each field-scale block was subdivided into the contacted and bypassed zones so that flash calculations could be done for each zone.

The concept of transport coefficients which take the fine-scale variations in the compositions and behaviour of the phases into account was introduced by Barker & Fayers, (1994). This pseudoisation technique is a modification of the DZM method. Transport coefficients together with pseudo relative permeability functions can be applied during upscaling of compositional simulation problems involving complex phase behaviours such as those in porous media having various length scales of heterogeneities. In their study, Thibeau et al., (1995) performed the dynamic upscaling of compositional flows by applying pseudo-relative permeability to upscale molar fluxes instead of volumetric fluxes, and the modified of the components' molar fluxes within each phase using transport coefficients. The reproduction the fine-grid fluid flow was done using dual-scale simulations (DSS), where only the cells where the pseudo functions are to be calculated are refined, instead of the conventional representative element volume (REV) simulations where the entire reservoir is finely gridded. Christie & Clifford, (1998) upscaled a process of lean gas injection into oil at residual saturation without the inclusion of pseudo relative permeability curves using the alpha factors method combined with a streamline simulator.

Jerauld (1998) presented a framework of for upscaling a multi-contact miscible water-alternating hydrocarbon gas tertiary flood modelled using a four-component limited-compositional numerical simulator. The approach applied pseudo relative permeability functions computed by a pore-volume weighted method, Stone's method of Stone (1991), and the total mobility method of Barker & Thibeau (1997) during the waterflood phase to match full-field, fine-grid fully-compositional reference simulations. Ajose & Mohanty, (2003) applied the α–factors method to upscale the flow of components in gas condensate reservoirs. The effects of fracture orientations, gravity, and capillary pressure on the alpha factors were also examined with their results showing that these effects were significant on alpha factors while diffusion effects were trivial. Li & Durlofsky, (2016) described an approach for upscaling two-phase oil-gas compositional formulations by iterating the transport coefficients to enhance the correctness of the upscaled coarse-scale model. They concluded that the compositionally upscaling approach can be applied to processes that require a wide range of simulation runs (at changing well operating parameters), such as uncertainty analysis, sensitivity studies and production optimization problems. In summary, these studies have shown that using upscaled alpha factors, particularly when they are appropriately tuned, during compositional upscaling is important and that the results are more

accurate when transport coefficients are incorporated with pseudo relative permeability functions. However, this process is computationally expensive, and is only halted when an appropriate match of the fine-scale result is obtained subject to the engineer's preference.

In this study, we sought to reduce the computational costs and reduce human efforts associated with upscaling of miscible displacements by applying an assisted upscaling method based on an Artificial Neural Network (ANN) coupled with a Genetic Algorithm (GA). This method was inspired by the idea of automatic or assisted history matching where the error between the observed and simulation predicted reservoir historical data is reduced using an optimisation algorithm (Alireza and D, 2012; Dang et al., 2016; Foroud et al., 2014; Zhang et al., 2012). First of all, accurate numerical simulations of miscible CO_2 floods in two SPE benchmark cases were performed on fine-scale grids. The solutions and flow characteristics of the fine-scale grids were upscaled to coarse grids using a technique based on the pseudoisation of relative permeability and transport coefficients of each component in the oil and gas phases as a function of the injected gas. This pseudoisation of relative permeability captures the field-scale volumetric fluxes of the phases while the transport coefficients accounts for small-scale molecular diffusion of the component within the oil and gas phases, and the phase behaviour.

To attain a suitable match of the dynamics of the fine-scale model, manual calibrations of the transport coefficients were firstly performed. This process was discovered to be time-consuming as multiple numerical simulations of the coarse-scale models were required. Therefore, the assisted upscaling method earlier described was implemented.

Methodology

Calculation of pseudo relative permeabilities

The pseudo relative permeability functions used in this study were computed using the mobility-weighted pseudoisation technique of Zhang & Sorbie, (1995). This approach does not require the computation of the conventional single-phase flow upscaling parameters such as the transmissibility (T^*) and the well index (WI^*). The effects of large variations in flow rates which typically occur as a field is being developed are considered by the mode and there are no flow rate limitations in this approach. The fluxes out of a coarse-scale block for calculating the pseudo functions are only computed once (Zhang & Sorbie, 1995). This results in a reduction of numerical dispersion, and the capture of the interactions of the fluid flow associated with fine-scale reservoir heterogeneity ensuring that the volumetric flows of the phase are accurately matched. The method is also effective for computing the pseudo

functions that approximate the fine-grid solutions and is more robust than the approach of Kyte and Berry, (1975) and other pore-volume-weighted methods. For example, these methods only derive pseudo-functions for flow in a single direction, while the method applied in this study can compute two- and three-directional pseudo-functions that suit highly anisotropic or flow-direction-dependent heterogeneous media.

This method has also proven to be effective when the capillary pressure and gravity effects are negligible (Zhang & Sorbie, 1995; Barker and Thibeau, 1997). In this study, the effects of capillary forces and gravity were neglected. The method is applicable to all flow rates even in non-communicating layers where the viscous-to-gravity ratio is infinite. To reduce the computational requirements of global upscaling while retaining the accuracy of global upscaling procedure, the pseudo functions were calculated using a local upscaling technique where the entire reservoir was fine-gridded, and a representative element volume (REV) of reservoir was applied to derive the required pseudo functions. This also eliminated the need of injecting thousands of pore volumes of the gas to cover the whole saturation range required to estimating the pseudo functions if a global upscaling was used. Using the local upscaling approach, the REV can experience the required overall saturation ranges at considerably smaller pore volumes of gas injected.

The pseudo functions were computed as functions of flow in the principal flow direction, the horizontal direction. Fig. 1 depicts a 2D → 2D upscaling case for a coarse-scale block containing ($i_8 - i_1$) x ($k_8 - k_1$) fine-scale grid blocks.

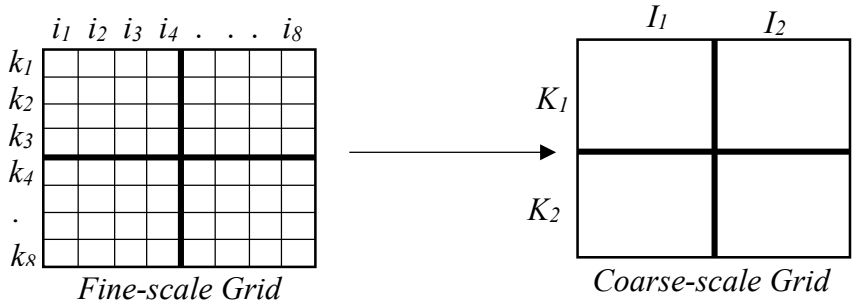

Fig. 1: A schematic of a *4* x *4* upscaling case for a 2D coarse block in Case 1.

The fine-scale and coarse-scale grid flowrate at the coarse grid boundary in the *x*-direction are equal and is given as:

$$\bar{q}_{t,x} = \sum_{k=k_1}^{k_4} (q_t)_{k,i4} \quad (1)$$

or

$$\bar{q}_{t,x} = \sum_{j=j_1}^{j_{10}} \sum_{k=k_1}^{k_5} (q_t)_{k,i5}, \text{ for a 3D reservoir model} \quad (2)$$

The average saturation of the phases within the coarse grid block, $\bar{S}_p$ is given as:

$$\bar{S}_p = \frac{\sum_{i=i_1}^{i_4}\sum_{k=k_1}^{k_4}(V_p S_p)_{i4,k}}{\sum_{i=i_1}^{i_2}\sum_{k=j_1}^{k_2}(V_p)_{i4,k}} \tag{3}$$

or

$$\bar{S}_p = \frac{\sum_{i=i_1}^{i_5}\sum_{j=j_1}^{j_{10}}\sum_{k=k_1}^{k_5}(V_p S_p)_{i5,k}}{\sum_{i=i_1}^{i_5}\sum_{j=j_1}^{j_{10}}\sum_{k=k_1}^{k_5}(V_p)_{i5,k}}, \text{ for a 3D reservoir model} \tag{4}$$

where V_p is the pore volume of the grid block. The fractional flow of the phase p in the x – direction out of a coarse grid cell is given as:

$$\bar{f}_{px} = \frac{\sum_{k=k_1}^{k_4}(\bar{q}_t f_p)_{i_4k}/\mu_{p,i_4k}(c_{i_4k})}{\sum_{k=k}^{k_4}(\bar{q}_t)_{i_4k}/\mu_{p,i_4k}(c_{i_4k})} \tag{5}$$

or

$$\bar{f}_{px} = \frac{\sum_{j=j_1}^{j_{10}}\sum_{k=k_1}^{k_5}(\bar{q}_t f_p)_{i_5k}/\mu_{p,i_5k}(c_{i_5k})}{\sum_{j=j_1}^{j_{10}}\sum_{k=k_1}^{k_5}(\bar{q}_t)_{i_5k}/\mu_{p,i_5k}(c_{i_5k})}, \text{ for a 3D reservoir model} \tag{6}$$

Where i, j, and k represent x –, y –, and z – directions, respectively, and μ_p is the viscosity of the phase, p. Given that the flood is miscible, the viscosity, μ_{p,i_nk} is a function of the solvent concentration, c_{i_nk}. The inclusion of this parameter could also extend this method to immiscible floods. In this case, the viscosity, μ_{p,i_5k} would be a function of the saturation, S_p of the phase, p. The denominators of Eqns. 5 and 6 define the total flow rates of the phases across the coarse grid boundary in the principal direction(s) of fluid flow, while the numerators represent the flowrates of phase, p out of the coarse grid cell (Zhang & Sorbie, 1995). A transmissibility-weighted averaging was applied to derive the mean total pseudo mobility in the x-direction, $\bar{\lambda}_{tx}$.

$$\bar{\lambda}_{tx} = \frac{\sum_{i=i_1}^{i_4}\sum_{k=k_1}^{k_4}(T_x\lambda_t)_{i4,k}}{\sum_{i=i_1}^{i_4}\sum_{k=k_1}^{k_4}(T_x)_{i4,k}} \tag{7}$$

or

$$\bar{\lambda}_{tx} = \frac{\sum_{i=i_1}^{i_5}\sum_{j=j_1}^{j_{10}}\sum_{k=k_1}^{k_5}(T_x\lambda_t)_{i5,k}}{\sum_{i=i_1}^{i_5}\sum_{j=j_1}^{j_{10}}\sum_{k=k_1}^{k_5}(T_x)_{i5,k}} \tag{8}$$

Finally, the pseudo relative permeabilities curves in the x-direction are then computed by joining the fractional flow and total mobility equations, as:

$$\bar{k}_{rp} = \bar{f}_{px}\bar{\mu}_p\bar{\lambda}_{tx} \tag{9}$$

where $\bar{\mu}_p$ is the volumetric-averaged phase viscosity computed from the fine grid blocks that constitute a coarse grid block. In summary, the *x*-direction was determined as the principal flow direction in Case 1, and the pseudo-relative permeability functions were calculated for this direction only. In Case 2, the *x*- and *y*- directions were identified as the principal flow directions, and the pseudo functions were generated accordingly.

The grid block horizontal and vertical permeabilities were upscaled to be geometric means of the fine grid block permeabilities using Eqs. 10 and 11, accordingly. This method of permeability averaging was preferred to harmonic averaging because if a high permeability contrast exists between the blocks, the harmonic average may underestimate the connectivity of the blocks at the interface as it tends to be biased towards lower values.

$$\bar{k}_x = \frac{i_4 - i_1}{\sum_{k=k_1}^{k_4}\left((k_4 - k_1)/\sum_{k=k_1}^{k_4} K_{xk}\right)_{i4}} \tag{10}$$

or

$$\bar{k}_x = \frac{(i_5 - i_1)*(j_{10} - j_1)}{\sum_{k=k_1}^{k_5}\left((k_5 - k_1)/\sum_{k=k_1}^{k_5} K_{xk}\right)_{i5,j}} \tag{11}$$

During the upscaling of absolute permeability, the permeability variation within the fine-scale model is made more homogeneous. Numerical dispersion is also increased by the increase in the grid block sizes in the longitudinal and transverse directions, and the level of mixing or molecular diffusion is reduced compared to the fine-scale model. Thus, an efficient upscaling procedure should be able to effectively reduce numerical dispersion and match the level of mixing in the fine-scale reference model. The numerical dispersion can be calculated as (Akinyele and Stephen, 2020):

$$D_{num} = \frac{v}{2}\left(\Delta x - \frac{v\Delta t}{\phi}\right) \tag{12}$$

where $v \approx |v| \approx v_x$ is the flux in the longitudinal direction. This assumption is valid when velocity in the transverse direction is small compared to that in the longitudinal direction. Δx is the grid-cell size, Δt is the time step, and ϕ is porosity.

The application of pseudo fractional flows to calculate the pseudo relative permeability ensures that the volumetric phase and component molar flowrates are accurately matched. The transmissibility weighting of the total pseudo-mobility also guarantees the adequate calibration of the pressure-dependent fluid properties. Eqs. 1, 3, 5, 7 and 10 calculate the pseudo-functions for the 2D models, while Eqs. 2, 4, 6, 8, and 11 present the pseudo-

functions of a three-dimensional model. The pseudo relative permeability curves were generated for two-phase (oil-water and oil-gas) flows, and the Stone II model was used to calculate the three-phase relative permeability functions.

Calculation of the transport coefficients

Transport coefficients are used to correlate the fluxes of the reservoir fluids out of a field-scale coarse grid block to the average compositions of the fluids in the said block (Barker et al., 2005; Barker and Fayers, 1994; Fayers et al., 2007). Their use modifies the fluxes of the components in the oil and gas phases to take sub-grid phase behaviour and flow interactions into consideration. Fine-grid simulations that incorporate small-scale details of the reservoir heterogeneity are applied to compute the alpha factors.

This study applied alpha coefficients that were obtained from the results of fine-scale models. To reduce the complexity of the upscaling process, these factors were computed for flow in the *x*-direction in the 2D model, and the *x*- and *y*- directions in the 3D model. The calculated transport coefficients were presented as a function of the overall mole fraction of the injected gas (z_{CO_2}). Fig. 2 presents a local two-coarse-block region showing the outflow boundary and the region within a coarse grid block. The light lines represent the fine grid, while the heavy lines show the coarse grid.

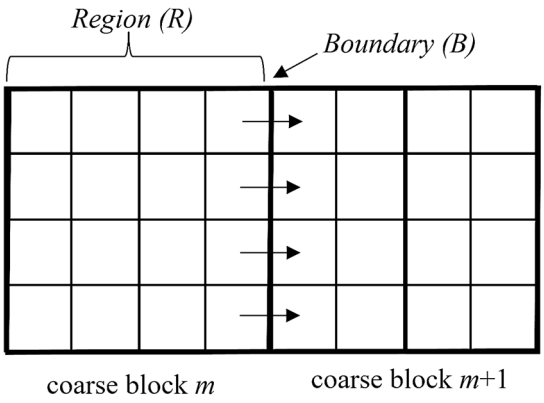

Fig. 2: A local two-coarse-block region showing the outflow boundary and the region within a coarse grid block. The light lines represent the fine grid, while the heavy lines show the coarse grid.

The procedure outlined below was employed for the computation of the transport coefficients:

- We specified a region *R* on the fine grid corresponding to one grid block in the coarse grid model. The outflow boundary at the interface of the region in the x-direction was labelled *B*, as shown in Fig. 3.
- At chosen time intervals, the molar flux (in mol per unit volume) of the component in the oil and gas phases out of the region *R* through the outflow boundary *B* was calculated (see Fig. 3). The flux of the components in the oil phase out of the region *R* was calculated as:

$$(\rho_o x_i)_B = \frac{\sum_B \Delta y \Delta z \rho_o u_{ox} x_i}{\sum_B \Delta y \Delta z u_{ox}} \tag{13}$$

$$(\rho_o x_i)_R = \frac{\sum_B \Delta x \Delta y \Delta z \rho_o u_{ox} x_i}{\sum_B \Delta x \Delta y \Delta z u_{ox}} \tag{14}$$

and flux of the components in the gas phase out of the region *R* was calculated as:

$$(\rho_g y_i)_B = \frac{\sum_B \Delta y \Delta z \rho_g u_{gx} y_i}{\sum_B \Delta y \Delta z u_{gx}} \tag{15}$$

$$(\rho_g y_i)_R = \frac{\sum_B \Delta x \Delta y \Delta z \rho_g u_{gx} y_i}{\sum_B \Delta x \Delta y \Delta z u_{gx}} \tag{16}$$

- We then calculated the transport coefficients as:

$$\alpha_{oi} = \frac{(\rho_o x_i)_B}{(\rho_o x_i)_R} \tag{17}$$

$$\alpha_{gi} = \frac{(\rho_g y_i)_B}{(\rho_g y_i)_R} \tag{18}$$

and then tabulated them vs. z_{CO_2}. The denominator defines the sum of these quantities over the fine grid cells (or region, *R*) that make up a coarse grid block. As usual, Eqs. 13, 15, and 17 compute the transport coefficients for the 2D models, while Eqs. 14, 16, and 18 present the transport coefficients for the three-dimensional model.

It is sometimes impractical to generate pseudo functions for every coarse block and flow direction in the upscaled models (Barker & Thibeau, 1997; Li & Durlofsky, 2016a). Therefore, in this study, we averted this expense by extracting a Representative Element of Volume (REV) and applied it to generate the pseudo functions in a process known as REV pseudoisation (Barker and Fayers, 1994; Barker and Thibeau, 1997; Jákupsstovu et al., 2001). We then grouped the coarse grid cells into several rock types based on the permeability value of the grid cell and assign the pseudo relative permeability and transport coefficient functions based on this grouping.

The upscaling of absolute permeability usually results in a decrease of permeability heterogeneity in the coarse-scale model as the resulting permeabilities are bias towards lower values. This, in turn, could result in an underestimation of recoveries in coarsened models due to the loss of small-scale reservoir heterogeneities. Also, there may be a difference between the pressures of the wells from the fine grid to the coarse grid, and the BHP of the producers may fall below the MMP, which is undesirable for miscible displacements. We tested the validity of the pseudoisation approach by carrying out the numerical simulations of single-phase flow in the first model. A close match of the pressures was obtained indicating an efficient absolute permeability upscaling.

Improving the Upscaling Results: Calibrating the transport coefficients

Manual Tuning

When performing the upscaling procedures described above, i.e., the pseudo-relative permeabilities and the transport coefficients, it was assumed that the quantities of the coarse-scale grids are the fine-scale averages. Although this assumption is reasonable, it does not always hold, as a mismatch between the phase fluxes of the integrated fine-scale and that of the coarse-scale is commonly encountered. However, the reliability of the upscaling results strongly depends on the proper calibration and the elimination of this mismatch. It is, however, possible to improve the accuracy of the upscaling results by tuning some of the derived upscaled coarse-scale quantities such as the alpha factors, absolute permeability or the end-points of the relative permeabilities as described by Barker and Thibeau, (1997), Chen et al., (2008), and Li and Durlofsky, (2016). The tuning, which is similar to that done in reservoir history matching, is done so that the differences between the fine- and coarse-scale models in terms of the phase and composition flowrates and/or any other performance metric are minimized or eliminated.

For the miscible flooding upscaling considered, preliminary sensitivity showed that calibrating the transport coefficients of CO_2 in the oil and gas phases, i.e., α_{o,CO_2} and α_{g,CO_2}, had the most significant impact on the accuracy of the results. The precedence of transport coefficients over pseudo relative permeability functions (k_r) during compositional upscaling has been reported by Li and Durlofsky, (2016a) and Zhang and Sorbie, (1995). Therefore, in this study, we carried out the tuning of the generated alpha functions. To achieve a suitable match of the fine grid model by the upscaled models, these quantities were calibrated by changing their values iteratively until suitable solutions was attained. However, we acknowledge that for other upscaling problems, iterating more coarse-scale quantities may be

helpful. Given the initial estimates of α_{o,CO_2} and α_{g,CO_2} computed from Equation 17 and 18, the coarse-scale compositional flow equations were solved. The flux of the component *i* in the phase *p*, $(u_{px}y_i)^c$ or $(u_{px}x_i)^c$ for the gas and oil phase, respectively, through the coarse interface was then calculated. Based on this mismatch, an updated α_{p,CO_2} was calculated as (Li and Durlofsky, 2016a):

$$\alpha_{p,CO_2}^{v+1} = d\alpha_{p,CO_2}^{v} + (1-d)\frac{\sum_B (u_{px}y_i)^f}{(u_{px}y_i)^c}\,\alpha_{p,CO_2}^{v} \tag{19}$$

where superscript *v* represents the current iterartion and *v+1* is the next iteration, *d* represents the damping which is used to prevent abrupt variations in α_{p,CO_2}^{v}. $(u_{px}y_i)^f$ is the total flux of the component in the gas phase across the boundary in the fine scale grids and can be interchanged with $(u_{px}x_i)^f$ for computations involving the oil phase. It was required that the time step be repeated within the coarse-scale simulation severally to obtain the coarse-scale parameters needed for Equation 19. About six iterations were performed to obtain a suitable match meaning that the process was relatively computationally expensive. This method of tuning transport coefficient instead of k_r is particularly effective in multi-contact miscible floods because relative permeability effects are minimal, and mass transfer between the phases is good, as is the case in this study.

To assess the accuracy of the solutions of the upscaled and the standard coarse models, the errors of the production rates of the phases and some selected components were calculated. The error was calculated as the relative error (RE) given as:

$$RE = \frac{1}{n}\sum_{i=1}^{n}\frac{\left|R_t^c - R_t^f\right|}{R_t^f}\ X\ 100\% \tag{20}$$

where R_t^c and R_t^f are the oil or gas production rates at timestep, *t* for the coarse and fine grids, respectively. Based on the computational expense, a relative error less than 10% is regarded as acceptable for this procedure.

Assisted calibration of the transport coefficients using an ANN-based optimisation routine

The procedure of calibrating the transport coefficients described in the previous section was only stopped when a suitable result was attained based on the engineer's discretion. This was a time-consuming process due to the multiple numerical simulations runs required to achieve this suitable match. To address this, we treated the calibration as a multi-objective optimisation problem where the objective(s) was the reduction of the mismatch between the predictions of the upscaled coarse-scale models and the fine-scale model. The proposed

methodology was evaluated on the upscaling of Case 1, knowing in advance that it would also work for Case 2.

The assisted upscaling workflow focuses on calibrating the transport coefficients using the observed predictions of the fine-scale model. It required solving an inverse problem for which the solution would be non-unique since many combinations of parameter settings would yield a similar model response. From the optimisation perspective, the calibration process can be defined as follows:

$$\min_{x \in \Omega} \|O(x) - y\|^2 \tag{21}$$

where $y \in R^m$ denotes the vector of measured observations from the fine-scale simulation and $O(x) \in R^m$ is upscaling solutions. x represents the optimisation variables which belong to feasible domain Ω. The objective of this inverse problem us to obtain an x such that the distance between the resulting upscaling outputs and the fine-gridded simulation is minimised. In summary, the optimisation variables in this problem were the transport coefficient of the components in the oil and gas phases, and the objective function was the minimization of the root mean-squared error (RMSE) between the predicted hydrocarbons phases, and components production rates. The RMSE of each quantity is given as:

$$\sigma_m = \sqrt{\frac{1}{N_d}\sum_{t=1}^{N_d}(e^{(t)})^2} \tag{22}$$

where, $e^{(t)} = \frac{R_c^t - R_f^t}{R_f^t}$, N_d is the number of the observed points; R_c^t and R_f^t are production rates of the metric, m considered for the, fine-scale and the upscaled coarse-scale models corresponding to timestep, t, respectively. Sixteen metrics were considered in the preliminary objective function, the total RMSE which is given as:

$$Total\ RMSE = \sum_{i=1}^{n}(\sigma_m), \quad n = 16 \tag{23}$$

The assisted calibration routine requires excessive costly full-physics simulations, and in most cases the derivative information is expensive to obtain or may not be available. Recent advances in computational capabilities have allowed the application of optimisation algorithms to assisted history matching problems. This framework can also be implemented in upscaling problems. In this study, we applied a meta-heuristic algorithm, the Genetic Algorithm to the optimisation framework. The GA is advantageous for multi-dimensional, nonlinear optimisation problems like the present one which could contain many local minima in which other non-evolutionary optimisation algorithms can get stuck. The GA also has the capabilities of convergence to the global minimum, adaptability with different types of

dynamic data, and is independent from forward model structure. This ensures that the selection of parameters can be estimated with flexibility.

The surrogate model of the objective function. To reduce the computation time, we applied experimental design to screen the input variables and coupled it with proxy modelling to construct an approximation model of the desired objective function. Experimental design and proxy modelling is a well-established approach in petroleum engineering, particularly in modelling reservoir performance (Agada et al., 2017; Aghbash and Ahmadi, 2012; Aghdam and Ghorashi, 2017; Dai et al., 2017; Karimaie et al., 2017). Their application of an efficient experimental design ensures that maximum information on the relationship between the objective function and the multidimensional optimisation variables is obtained at minimum expense. In combination with approximation models, they can be used for sensitivity analysis and for approximating the objective function. The approximated objective function can then be optimised using a reasonable optimisation algorithm. An extensive review of experimental design and proxy modelling techniques and their suitability for optimisation problems has been carried out by Ogbeiwi et al., (2020).

Data-driven proxy modelling techniques together with experimental designs such as Box-Behnken, central-composite, fractional factorial, Latin-hypercube designs, etc., such as artificial neural networks are applied in petroleum engineering to construct an approximation model of the desired objective function (Costa et al., 2014). An extensive review of experimental design and proxy modelling techniques and their suitability for optimisation problems has also been carried out by Ogbeiwi et al., (2020). In this study, we applied an artificial neural network (ANN) to construct approximation models of the desired objective function. To ensure that the constructed data-driven proxy model fully explores the parameter spaces of the input variables, a space-filling Latin Hypercube Design (LHD) was used to construct the simulation runs needed to construct the approximation model.

ANNs are information processing systems which approximate biological neural network systems. They consist of numerous artificial neurons that are highly interconnected and serve as processors, and are generally characterized by the amount of neurons and layers, and their connectivity (Negash et al., 2017). The correlations between the inputs and outputs are modelled using the neurons and their connectivity weights. In this study, the ANN training task was done by setting the weights and biases of the network so that it approximated the RMSE derived from the responses of the full-physics numerical simulation models.

A feed-forward backward propagation multi-layered neural network (BPNN) architecture was applied in this study. Unlike other ANN architectures such as the feed-backward and the

self-organizing neural networks, a feed-forward NN containing only one hidden layer with enough neurons in this layer can adequately fit any finite input-output fitting problem (Negash et al., 2017). The interested reader is referred to Foroud et al., (2014) and Negash et al., (2017) for more understanding of these concepts. We also specified a tangent-sigmoid transfer function for the ANN.

Using the design obtained from the Latin-Hypercube design, ninety-six full-physics numerical simulations and computations of the objective function were performed to train the NN model. The BPNN architecture was implemented in MATLAB (Mathworks Inc, 2019) so that the input layer of the NN model contains 16 layers corresponding to the number of input variables. A hidden layer containing 20 neurons was specified to connect to the input layer by weights and a transfer function:

$$a_i^1 = tansig(y_i + b_i^1),\ i = 1 - 20 \tag{24}$$

$$with:\ y_i = \sum_{j=1}^{20} X_{ij}\,;\quad X_{ij} = X_j\ .\ w_{ij}^1 \tag{25}$$

where X_{ij} is the variable in the input layer, w_{ij}^1 represents the corresponding weight of the *j*th neuron of the input layer that connects with the *i*th neuron of the hidden layer, and b_i^1 is the bias value of the i^{th} neuron in the hidden layer. A tangent-sigmoid transfer activation function was specified as follows:

$$tansig(x) = \frac{2}{1+ e^{-2x}} - 1 \tag{26}$$

The choice of these parameters was informed by a sensitivity analysis conducted to predict the optimum values of these parameters. In the ANN model, the backpropagation algorithm initiates the vectors of the initial weights and bias values from which the feedforward network calculates the output. The accuracy of the estimation was measured as the error between the actual RMSEs, and the proxy predicted RMSEs. The weights and biases of the ANN model are adjusted throughout the training process using the Levenberg-Marquardt algorithm. As this adjustment is carried out, a more accurate model can be typically obtained when a larger volume of data is used in the training routine.

The accuracy of the NN model was validated using the coefficient of determination (or the R^2 goodness of fit). Fourteen additional simulations/ evaluations of the objective function were used to test the accuracy of resulting NN model.

The R^2 goodness of fit is given as:

$$R^2 = 1 - \frac{SS_{res}}{SS_{tot}} \tag{27}$$

where $SS_{tot} = \sum_{i=1}^{N_d}[|{y_t}^{(i)} - \bar{y}_t|]^2$ is the total sum of squares, and represents the sum of the

variation of the experimental values around its mean value($\overline{y}_t$), and $SS_{res} = \sum_{i=1}^{N_d}[|e^{(i)}|]^2$ is the residual sum of squares.

The Optimisation Algorithm. The main objective of the assisted upscaling process is to find the value of the transport coefficients that result in a minimum RMSE. The genetic algorithm (GA) in MATLAB (Mathworks Inc, 2019) was implemented in a closed loop with the objective function for this purpose. The GA develops a generation of candidate solutions according to the given problem using operators that copy natural genetic variation and natural selection. It consists of selection, recombination and mutation acting on individual solutions that are decoded and evaluated for fitness. The GA is commonly apply in global search for optimal solutions where there is limited knowledge about the distribution of the input variables (Foroud et al., 2014).

The GA operators used in the optimisation routine are presented in Table 1. The tolerance function states the required difference between the new and existing optimal values and the optimisation routine is terminated when the defined value is achieved. A mutation probability of 5% per model was applied to allow the algorithm to sample a broader search space and avoids being struck at the local minima. According to Minton (2012), these choices are conventional for any optimisation using a GA.

Table 1: Optimisation algorithm operators

Population	50
Maximum generations	50
Mutation probability	5%
Tolerance function	$1x10^{-6}$

In the closed-loop approach, a closed loop is formed between the optimiser engine, the GA and the trained ANN as the fitness function evaluator, and the GA attempts to find the minimum RMSE obtained by the ANN. Since the GA is a stochastic search algorithm, the optimisation search in each iteration is repeated Three iterations of the optimisation experiment were performed to ensure that a global optimum solution was obtained. As a stochastic search method, the GA searches for the optimal variables in each iteration using a different initial population, and the values at the final iteration were taken as the optimal results. However, the law of diminishing returns when optimizing the GA is also acknowledged, as the proxy model is very fast to evaluate. Our main concern however is to

reach the global optimum rather than do it as fast as possible.

The result from the optimisation routine was validated by applying it to the numerical simulator. If the NMSE obtained was unsatisfactory, the result was added to the training data set and the ANN was retrained. This process was repeated until a termination criterion, which is that a suitable RMSE with a relative percentage error of 1.5%, is reached. By doing this, the accuracy of the ANN particularly around the region of the optimal solutions was improved, and the optimisation algorithm was not stuck in a local optimum. The performance of this model on the training and testing data is shown in Fig. 3.

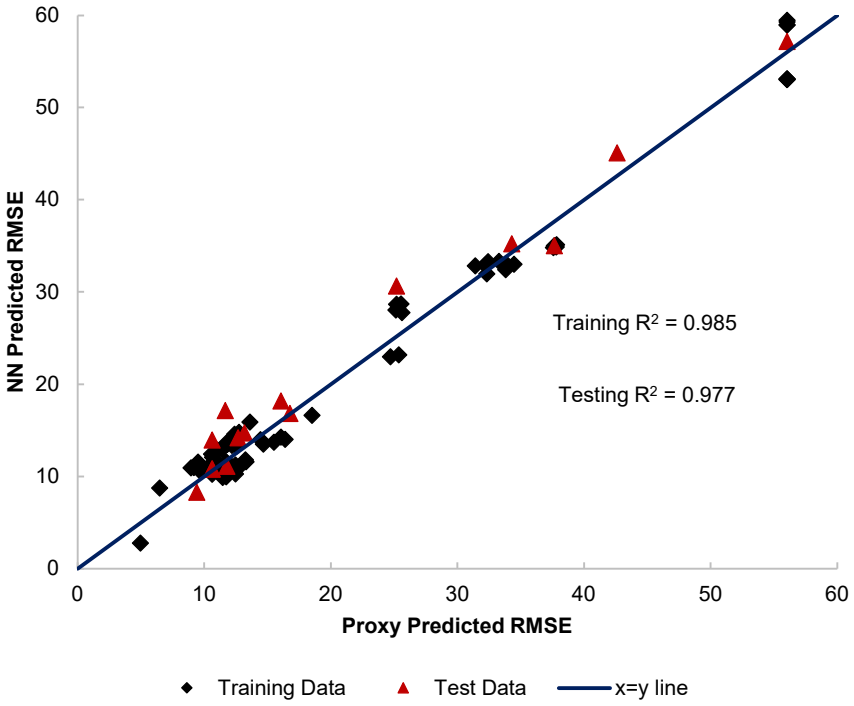

Fig. 3: Parity plot of the simulation predicted vs. the NN predicted RMSE.

In summary, the assisted-calibration upscaling technique serves two purposes: reducing human effort by supporting the human (or engineer's) judgement with well-developed mathematical method (using the optimisation algorithm) and saving computational cost by taking advantage of proxy modelling to decrease the numerous numerical simulations of the reservoir.

In conclusion, the upscaling methodology applied can be summarised as follows:

- Performing fine-scale full-physics simulations of the CO_2 miscible flood.
- Pseudoising the relative permeability function and the transport coefficients.
- Tuning the transport coefficients to eliminate the error between the fine- and coarse-scale results.

- GA-assisted automatic tuning of the transport coefficients for faster upscaling.

Results and Discussion

Case Study Examples: Reservoir Model Descriptions

We tested the proposed methodologies on two case study reservoir models which are available in the literature. They are a two-dimensional cross-sectional model, and quarter-five spot three-dimensional model extracted from a sector of Case 2, of the 10th SPE Comparative Solution Project on Upscaling (Christie & Blunt, 2001). Vertical production and injection wells were applied in both scenarios. Other assumption made include that there were no chemical reactions and gravity. The assumption of negligible gravity effects is reasonable for reservoirs were heterogeneity dominates the flow patterns as in the case in both reservoir models (Chang et al., 1994; Garmeh and Johns, 2010). Negligible adsorption or dissolution of CO_2 in the in-situ water was also assumed and the effects of relative permeability hysteresis is neglected. The top and bottom boundaries of the reservoirs are no-flow boundaries. The injection wells are at constant rate, while the producers are operated at constant pressures. The injection of CO_2 in a secondary flood in both cases were carried out after a waterflood carried out to bring the oil saturation to a residual value. The injection rates were 1.5 PV/year in Scenario 1 and 0.2 PV/year in Case 2. The fluid system in both cases was adapted from P Ogbeiwi et al., (2020) and corresponds to a miscible displacement. A uniform and constant porosity was assumed in the Case 1. The properties of these case studies are summarized in Table 2.

Table 2: Properties of the reservoir models

Property	***Case 1***	***Case 2***
Fine-scale grid discretisation	100 x 1 x 20 (2000 cells)	30 x 110 x 35 (115,500 cells)
Coarse-scale domain dimensions	25 x 1 x 5 (125 cells)	6 x 11 x 7 (462 cells)
Average horizontal permeability, k_H (mD)	162.9	218.36
Average vertical permeability, k_V (mD)	162.9	58.60
Reservoir thickness, (ft)	12	35
Average porosity, fraction	0.3443	0.182
Average fine Grid cell size (ft)	5 x 70 x 0.6	10 x 10 x 1
Model dimensions (ft)	500 x 70 x 12	300 x 1100 x 35

Anisotropy (k_V/k_H)	1.0	0.27
Oil viscosity, cP	1.33	1.33
Water viscosity, cP	0.613	0.613
Water viscosity, cP	0.175	0.175
Anisotropy (k_V/k_H)	1.0	0.27

Case 1: SPE comparative solution project model 1

The first model was a three-phase 2000-cell 2D vertical cross-sectional model with no dipping or faults. The dimensions were 500ft long x 70ft wide x 12ft thick. The size of the fine-scale grid is 100x1x20, with a uniform size for each grid block. The porosity and permeability distributions across the reservoir were derived from the 10th SPE comparative solution project model 1 (Christie & Blunt, 2001). The continuous injection of CO_2 was performed for 180 days with the injector well controlled at a target bottomhole pressure (BHP) of 3000 psi (and at 580 SCF/day). These conditions ensured that the reservoir pressure was maintained above the minimum miscibility pressure (MMP =1160psia) to guarantee the miscibility of CO_2 with oil throughout the flood. The production well was operated at a target oil flowrate of 100 STB/day and a minimum BHP of 3000psia was specified. The directional permeabilities are equal such that $k_x = k_z$.

The 2D, 100 x 20 fine model was coarsened to a 25x5 2D model (see Fig. 2). The pseudo functions were calculated for representative cells (an REV), comprising a local region comprising of the grid blocks that lie at the centre of the model (i = 52 and i = 60), and for each vertical grid block in this region (i.e., k = 1 to k =20). Five groups of the coarse-scale reservoir model permeability were identified. The derived pseudo functions was applied to the upscaled full-field grid blocks based on the permeability within each block as prescribed by Christie and Clifford, (1998). Fig. 4 shows the permeability distributions of the fine and that of the upscaled coarse model derived from the geometric averaging of the fine-scale model.

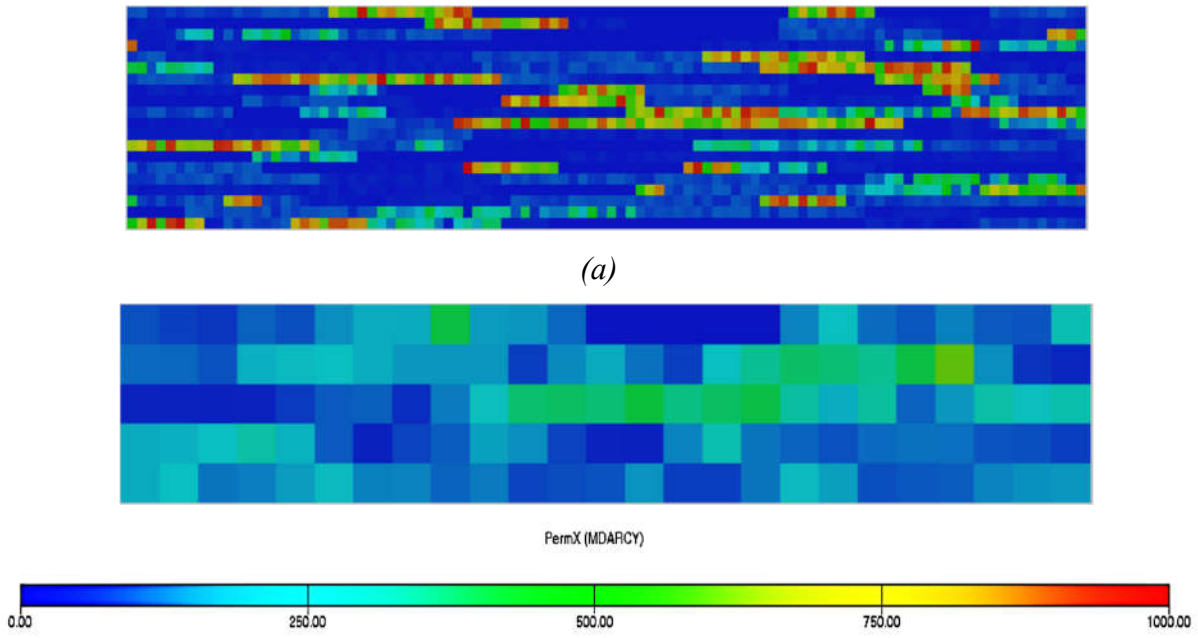

(a)

(b)

Fig. 4: Permeability distributions of the (a) fine and (b) upscaled coarse model.

The discretisation of the continuum equation gives rise to inherent errors due to differences between the discrete and continuum equations which are functions of the discretization method and the grid resolution (fineness or coarseness). Furthermore, the effects of un-upscaled coarsening and refining on the formation of viscous fingers can only be clearly defined in the fine-scale simulations. Discretisation errors increase with grid coarsening, and as such, we expect that there will be a mismatch between the solutions of the fine-scale and coarse-scale grids. It should be noted that this effect may be attributed to some level of physical dispersion, particularly in the finer grids where numerical effects are minimal. The numerical dispersion in the resulting models were calculated using Equation 12. The input, and the computed pseudo relative permeability curves of one of the five regions is shown in Fig. 5, while the final version of the calibrated transport coefficients of each component for each region is shown in Table 3. The capillary functions are set to zero and thus its effects are not included in the upscaling approach.

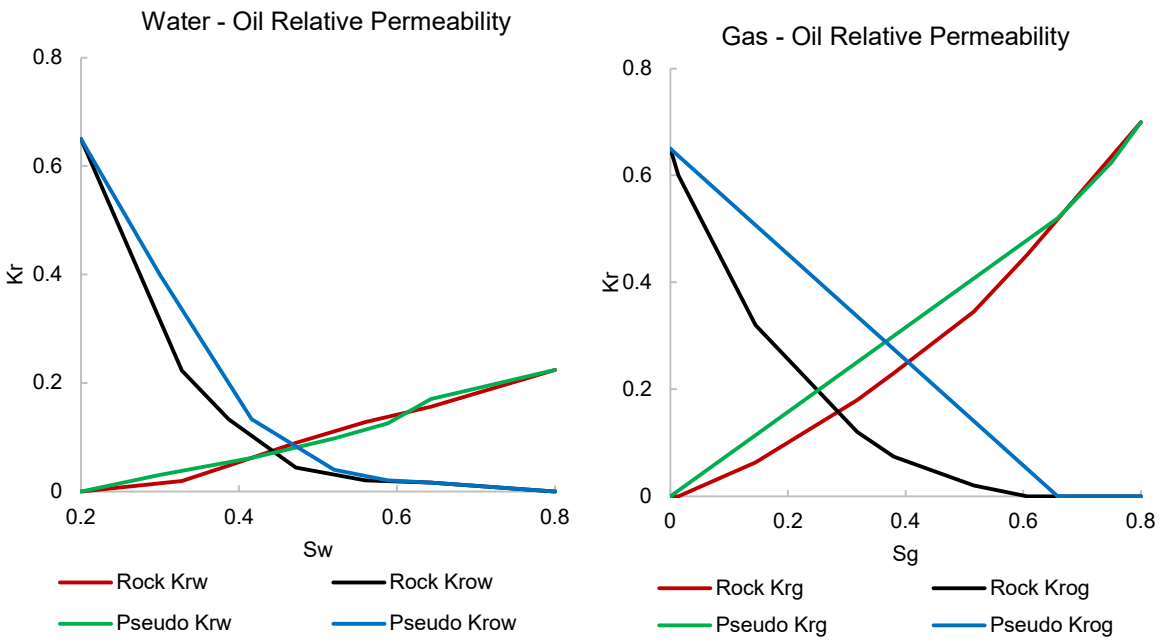

(a) *(b)*

Fig. 5: Example of the (a) water-oil, and (b) gas-oil rock and pseudo relative permeability curves.

Fig. 6 shows the distribution of CO_2 in the fine and coarse models at 0.65 PV of CO_2 injected. The displacement front was unstable as channelling due to heterogeneity act strongly, particularly in the fine-scale model (Fig. 6a). This causes the injected gas to avoid the low permeability zones of the reservoir, particularly at the top and bottom-right portions, and flow through the high permeability streaks in the reservoir.

Table 3: The calibrated transport coefficients of each component for each permeability group computed for Case 1.

z_{CO_2}	α_{o,CO_2}	$\alpha_{o,C1}$	$\alpha_{o,C2-nC4}$	$\alpha_{o,iC5-nC6}$	$\alpha_{o,HYP1}$	$\alpha_{o,HYP2}$	$\alpha_{o,HYP3}$	α_{g,CO_2}	$\alpha_{g,C1}$	$\alpha_{g,C2-nC4}$	$\alpha_{g,iC5-nC6}$	$\alpha_{g,HYP1}$	$\alpha_{g,HYP2}$	$\alpha_{g,HYP3}$
Group 1														
0.0118	1.684	1.254	1.003	1.003	1.003	1.003	1.003	2	1.25	1	1	1	1	1
0.687	1.75	1.448	1.154	1.138	1.089	1.165	0.759	1.986	1.45	1.152	1.139	1.12	1.114	1.151
0.866	1.996	1.258	1.006	1.005	1.002	1.006	0.893	1.998	1.398	1.117	1.111	1.088	1.063	1.042
0.962	2	1.273	1.008	1	1.009	1.02	0.999	2	1.335	1.077	1.1	1.154	1.136	1.006
0.974	2.01	1.25	0.986	0.91	1.002	1	1.005	2	1.259	1.006	1.006	1.006	1	1.001
Group 2														
0.0118	2.28	1.138	0.91	0.909	0.906	0.902	0.877	2	1.25	1	1	1	1	1
0.696	1.068	1.733	1.382	1.373	1.346	1.422	1.297	1.984	1.395	1.118	1.114	1.066	1.054	1.113
0.915	2	1.25	1	1	1	1	1	1.966	4.626	3.516	3.133	2.296	1.636	2.14
0.961	2	1.25	1	1	1	1	1	1.99	5.361	4.499	4.893	5.386	4.116	1.183
0.985	2	1.25	1	1	1	1	1	2	2.081	1.667	1.668	1.679	1	1.004
Group 3														
0.0118	2.31	1.118	0.895	0.897	0.901	0.904	0.903	2	1.25	1	1	1	1	1
0.73	2.05	0.894	0.785	0.915	1.101	0.859	1.363	2.016	1.116	0.909	0.935	0.957	0.957	0.873
0.913	2	1.25	1	1	1	1	1	2.006	0.923	0.738	0.748	0.815	0.882	0.928
0.962	2	1.25	1	1	1	1	1	1.998	1.781	1.444	1.47	1.45	1.196	1.022
0.976	2	1.25	1	1	1	1	1	2	1.478	1.183	1.186	1.201	1	1.001
Group 4														
0.0118	1.68	1.259	1.007	1.007	1.007	1.007	1.008	2	1.25	1	1	1	1	1
0.612	2.02	1.1	0.926	0.99	1.068	0.901	1.166	1.996	1.266	1.014	1.013	1.012	1.013	1.035
0.847	2.096	0.58	0.511	0.606	0.847	0.867	1.449	2.012	1.093	0.876	0.883	0.915	0.969	0.912
0.959	2	1.25	1	1	1	1	1	2.002	1.09	0.873	0.876	0.884	0.906	0.98
0.982	2	1.25	1	1	1	1	1	2	1.164	0.932	0.936	0.947	1	1
Group 5														
0.0118	2	1.25	1	1	1	1	1	2	1.25	1	1	1	1	1
0.158	1.14	1.31	1.049	1.05	1.053	1.055	1.062	2	1.25	1	1	1	1	1
0.677	2.126	1.085	0.867	0.861	0.842	0.72	0.745	1.95	1.388	1.11	1.11	1.11	1.123	1.226
0.926	2	1.25	1	1	1	1	1	2	1.228	0.986	0.996	1.023	1.031	1.004
0.985	2	1.25	1	1	1	1	1	2	1.131	0.905	0.906	0.91	1	0.993

The distribution of CO_2 concentration of fine-scale averaged onto the coarse-scale using a pore-volume weighted averaging was done to allow a more direct comparison with the upscaled and coarse model (as shown in Fig. 6b). The upscaling results show that the effects of gas channelling were better represented on the upscaled coarse-scale grids obtained using the iterated alpha factors and pseudo relative permeabilities displayed in Fig. 6c. The level of agreement of the CO_2 distribution in the fine-scale grid (Fig. 6a and 6b) to that of the procedure involving the calibrated alpha factors (Fig. 8c) was good illustrating the accuracy of the upscaling procedure over the full solution domain.

However, in the case involving non-calibrated alpha factors (Fig. 6d), the distribution of CO_2 was clearly overpredicted over a large portion of the model relative to the reference model (Figs. 6a and 6b). This was because while the pseudoisation of relative permeability alone guaranteed that volumetric phase fluxes were accurately matched, the use of the efficiently tuned alpha factors ensured that small-scale sub-grid heterogeneities and fluid interactions such as the molar diffusion of the components were better captured on the upscaled coarse-scale grids.

The effect of numerical dispersion was also observed when the grid blocks were coarsened without upscaling, which causes the CO_2 being distributed through the reservoir to be less dispersed in the coarse-scale models. This results in the incorrect splitting of the phases and components within a coarse grid block. The pseudoisation of the relative permeability and transport coefficient functions is clearly seen to reduce these effects as shown in **Table 4**.

Table 4: Reduction of numerical effects by the upscaling procedure

Scenario	Cells	Δx (ft)	Δt (days)	D_{num}
Fine-scale full-physics simulation	100 x 1 x 20	4	5	0.0705
Coarse-scale full-physics simulation	20 x 1 x 5	20	5	0.463
Upscaled (No Tuning)	20 x 1 x 5	20	5	0.32
Upscaled (+ Tuning)	20 x 1 x 5	20	5	0.104

In summary, a better match of the fluxes of the phases and that of the components in the oil and gaseous phases, as well as the pressure distribution were better matched when relative permeabilities and transport coefficients were pseudoised. As a result, the effects of small-scale sub-grid level viscous fingering and macro-scale channelling due to permeability

heterogeneity were better characterized by the application of pseudo relative permeabilities and transport coefficients to the upscaling procedure.

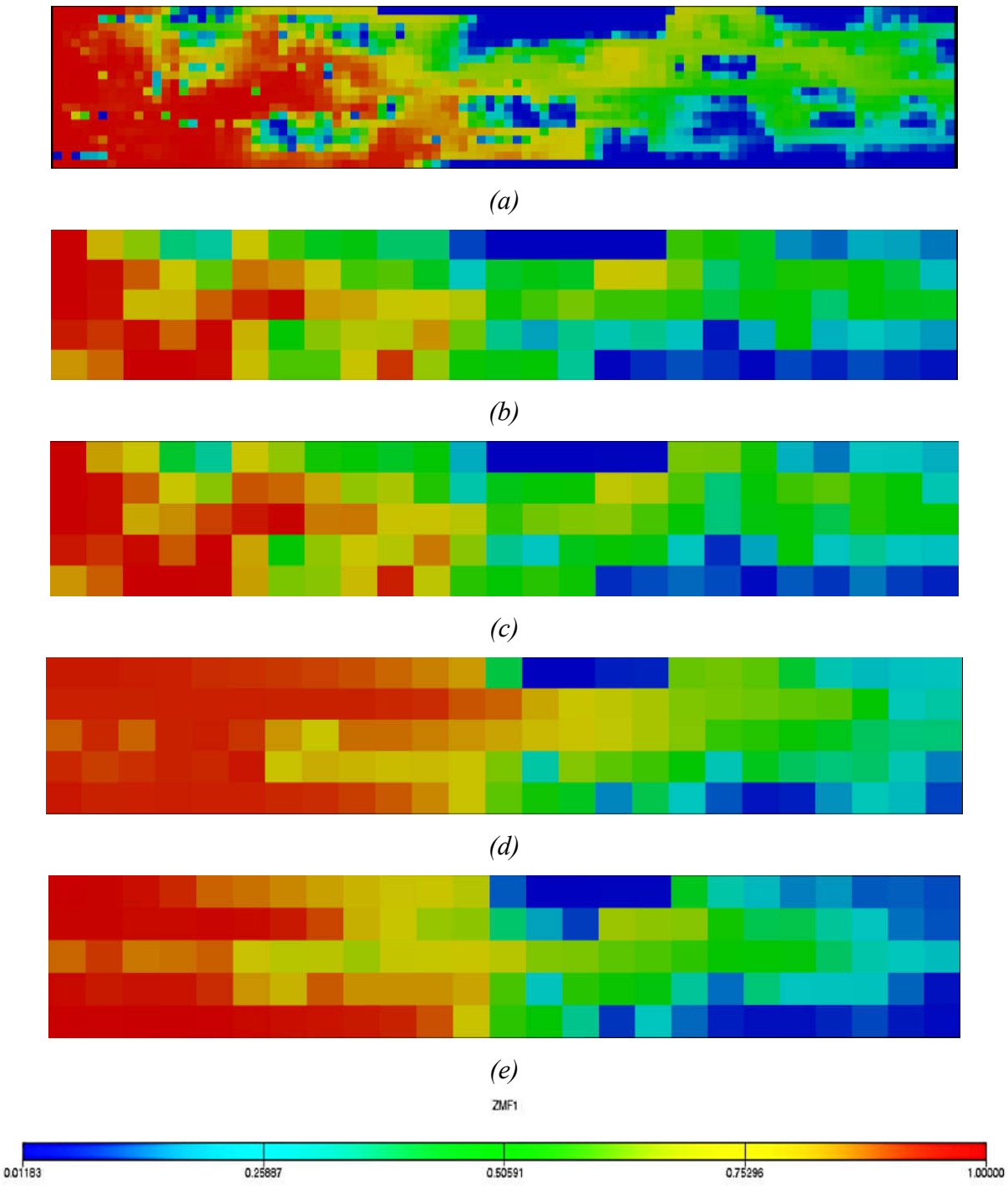

Fig. 6: Concentration of CO_2 at 0.65 PVI in the (a) fine-scale grid, and the coarse-scale grids where (b) the fine-scale composition were pore-averaged onto the coarse-scale grid, (c) iterated alpha factors were used, (d) non-iterated alpha factors were used, and (e) pseudoisation was not done.

Fig. 7 shows the fine and coarse grid recovery curves and compares the recoveries of the fine grid simulation (black line), the standard un-upscaled coarse model (green dotted line), and the upscaled models (blue and red-dashed lines).

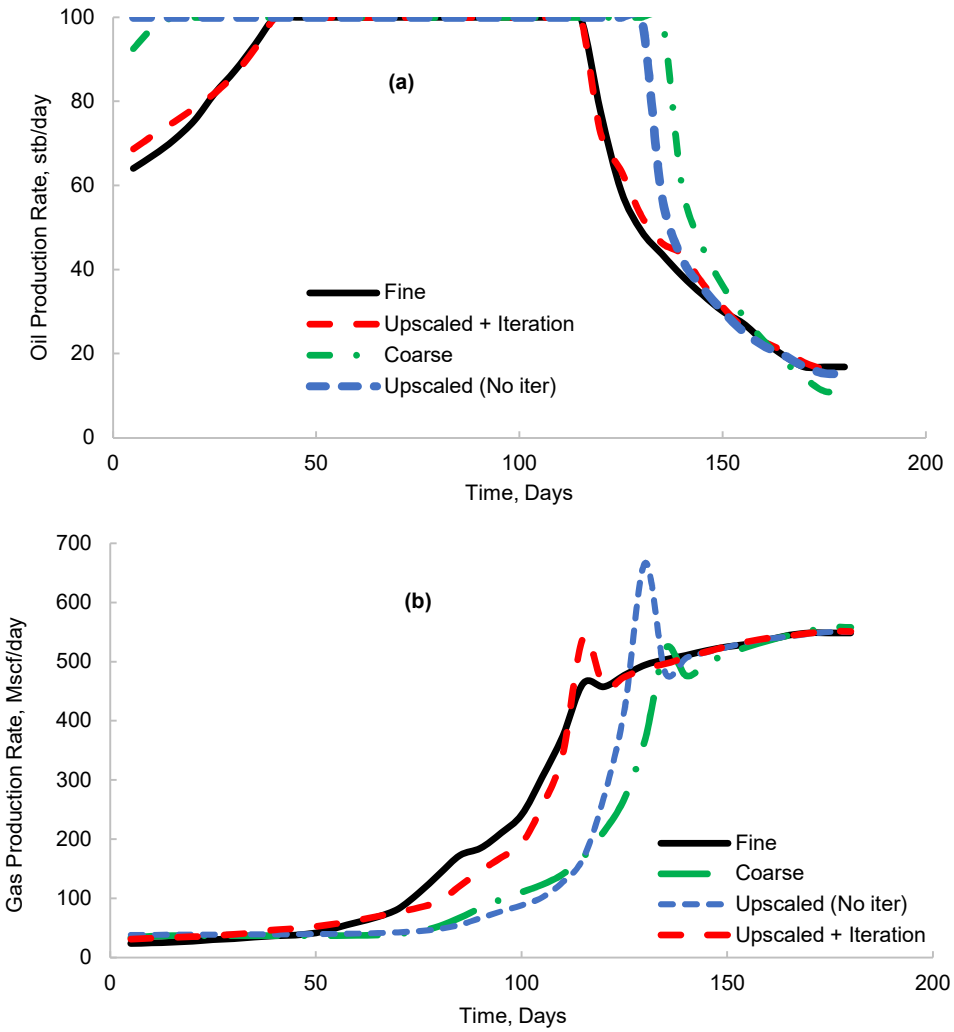

Fig. 7: Fluid production profiles of the fine and the upscaled coarse grids showing (a) oil recovery efficiency, and (b) gas production rate.

The figure shows a good level of agreement between the oil and gas production rates of the fine-scale model and the upscaled model where the alpha factors were tuned. However, the results of the standard coarse and the non-iterated upscaled models showed significant level of deviations from the production profiles of the fine-scale model. A calculation of the relative errors, RE, was done using Eq. 18 to quantify the errors of the solutions of the upscaling procedure by comparing the solutions of the different coarse-scale models to that of the fine-scale model. Based on the results obtained, the coarsening of the fine grids without upscaling led to significant inaccuracies in both the oil and gas production rates. However,

applying the tuning procedure produced the best results, with an RE of 2.28% for the oil rate and 13.6% for the gas rate.

We also considered the production rates of the individual components in the oil and gas phases rather than only the production rates of the phases. The fraction of CO_2 in the produced gas phase and that of the 4th component ($iC_4 – C_6$) in the produced oil phase are shown in Fig. 8.

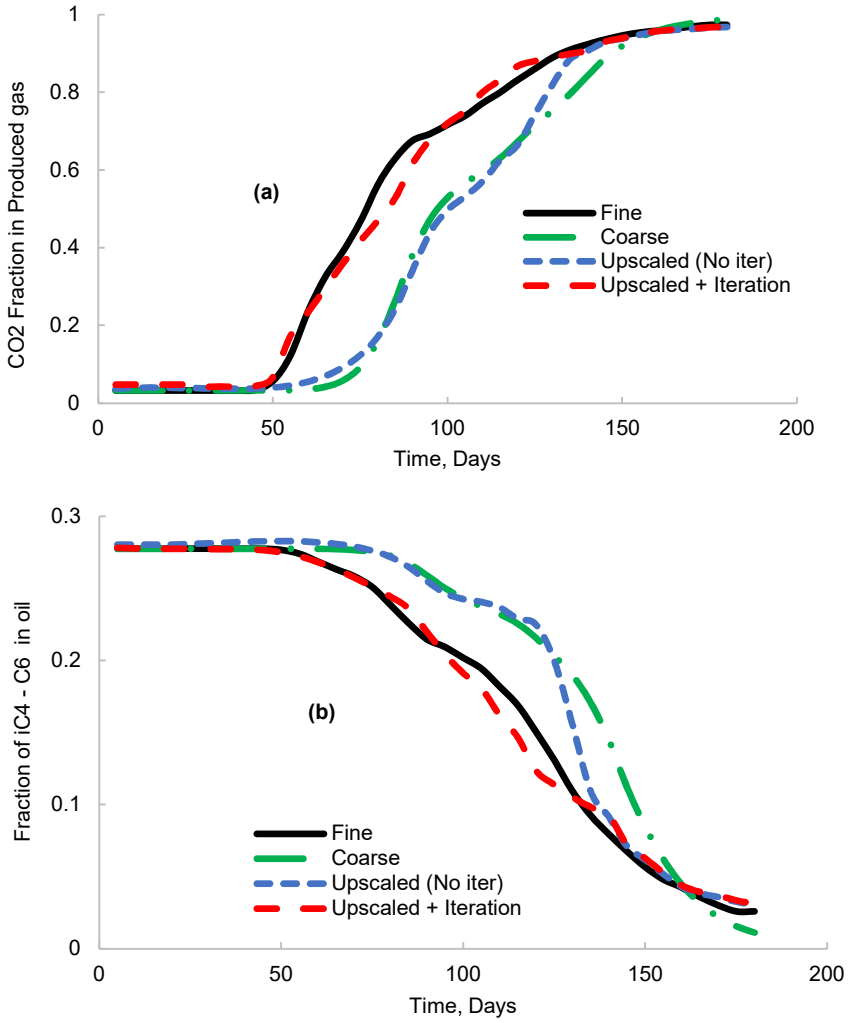

Fig. 8: Composition of (a) CO_2 in the produced gas, and (b) the 4th component (iC_4 - C_6) in the produced oil phase, of the fine and the upscaled coarse grids.

Since 100% of the injected gas is CO_2, we observed a sharp rise in the fraction of CO_2 in the produced gas after breakthrough, until almost all the produced gas is CO_2. Also, the profiles of the $iC_4 – C_6$ were very similar to that of the oil production rate profile because the component was produced with oil. The relative errors of the oil and gas production rates, as well as the fractions of CO_2 and the 4th component ($iC_4 – C_6$) in gas and oil, respectively, for model 1, are presented in Table 5.

Table 5: Summary of the errors of the upscaling results of the model 1

Simulation Model	Coarse	Upscaled (No Tuning)	Upscaled (+ Tuning)
Oil Production Rate	20.66%	13.97%	2.28%
Gas Production Rate	29.31%	30.46%	9.6%
CO_2 in gas	23.34%	25.72%	9.89%
$iC_4 – C_6$ in oil	22.98%	13.71%	6.16%

Just like the oil and gas production rates, there was also good agreement between the fine-scale simulation and the upscaled coarse-scale simulation involving the tuned transport coefficients. However, this was not the case for the standard coarse and upscaled models that do not incorporate the use of the tuned alpha functions.

Case Study 2: SPE comparative solution project 2

This case consists of a three-dimensional model with a simple geometry having no dipping or faults. This reservoir model's permeabilities and porosity distributions are obtained from a quarter-spot pilot of the Tarbert Formation, which is presented in the 10th SPE comparative solution project 2 (Christie & Blunt, 2001). The porosity distribution of this model is shown in Fig. 9. The model's dimensions were 300ft long x 1100ft wide x 35ft thick. The size of the fine-scale grid is 30 x 110 x 35 cells (115500 cells). The continuous injection of CO_2 into the reservoir was performed for 900 days with the injector well controlled at a fixed BHP of 3000 psi (and at 1160 SCF/day) to ensure that the flood was miscible, while the production well was operated at a constant oil flowrate of 200 STB/day (and a BHP of 1250psia).

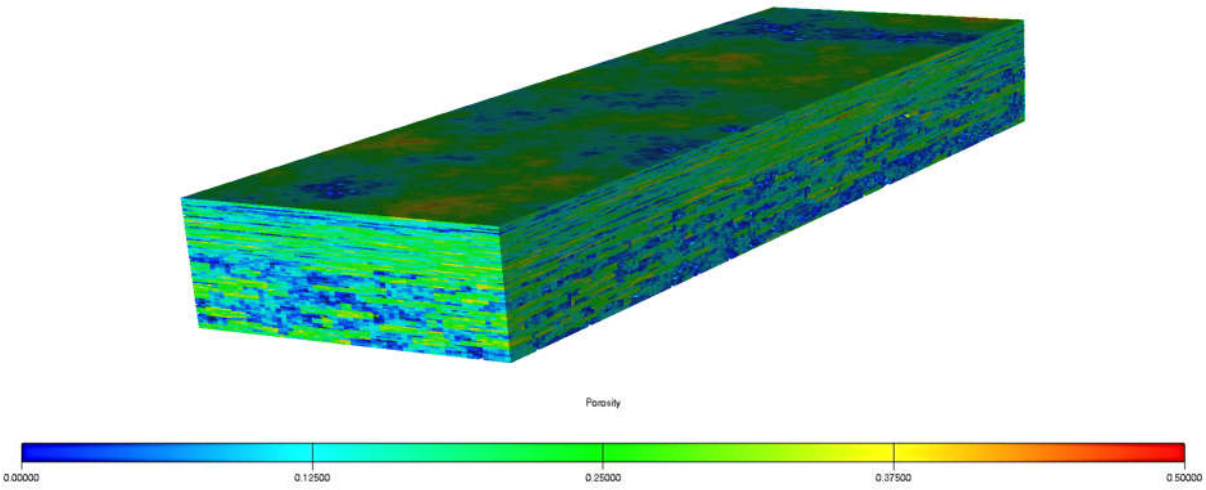

Fig. 9: The porosity distribution in Model 2.

We constructed the upscaled models by uniformly coarsening the fine-scale model by a factor of 10 in the *x*- and *y*- directions, and 5 in the vertical direction. Therefore, the coarse-scale model has a size of 6 x 11 x 7 = 462 grid cells. The fluid flow occurred predominantly in the horizontal direction, and flow in the *z*-direction, driven by gravitational effects, was neglected in this case. Therefore, calculating the pseudo-relative permeability functions and alpha factors in the *z*-direction resulted in many numerically correct but unphysical (i.e., negative) values. This phenomenon was also reported by Li and Durlofsky, (2016) and is attributed to occur because both integrated fluxes and averaged potential are small (Barker & Thibeau, 1997). Thus, we neglected the calculations of pseudo functions in the *z*-direction, as gravity is also deemed to be negligible. For studies where gravity is present or where there are strong vertical effects, such as in the vicinity of horizontal wells, the computation of the pseudo functional for the *z*-direction interfaces may be necessary.

Similar to the procedure used in Case 1, the pseudo functions were calculated for representative cells (REVs) and the values derived were applied to the upscaled global grid based on a permeability heterogeneity or rock type criterion. The computed pseudo relative permeability curves of seven rock types are shown in Fig. 10. The *x*-directional transport coefficients derived from the calibration procedure are presented in Table 6. The directional relative permeability curves and transport coefficients were specified in the coarse-scale simulation using relevant keywords of the ECLIPSE 300 compositional simulation software.

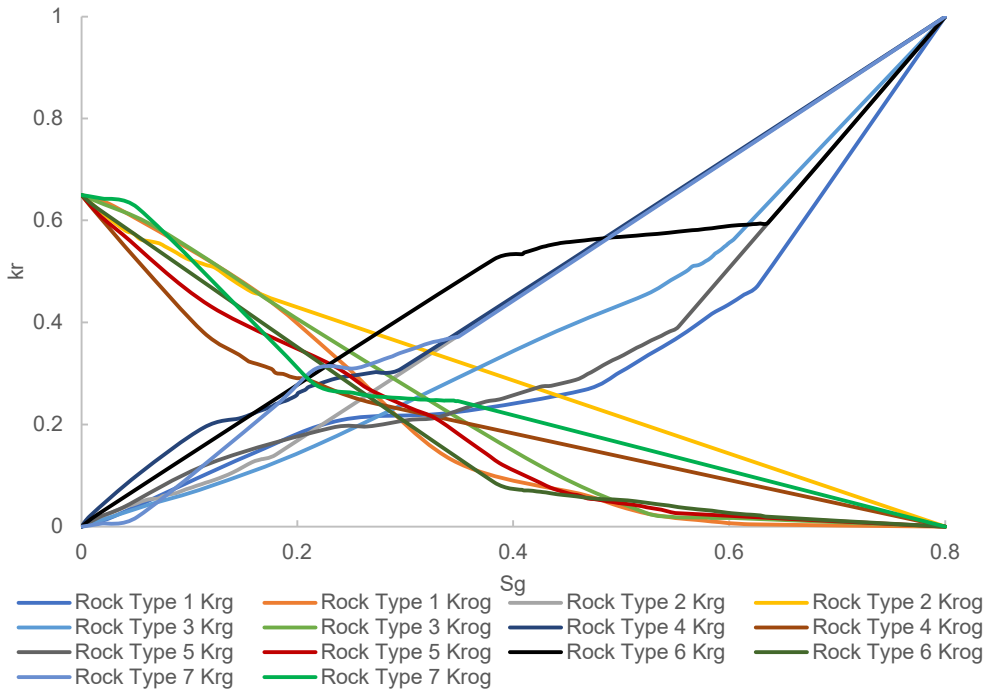

Fig. 10: The pseudo relative permeability curves of the seven rock types considered.

Table 6: The calibrated x-directional transport coefficients of each component applied in the upscaling of Case 2.

z_{CO_2}	α_{o,CO_2}	$\alpha_{o,C1}$	$\alpha_{o,C2-nC4}$	$\alpha_{o,iC5-nC6}$	$\alpha_{o,HYP1}$	$\alpha_{o,HYP2}$	$\alpha_{o,HYP3}$	α_{g,CO_2}	$\alpha_{g,C1}$	$\alpha_{g,C2-nC4}$	$\alpha_{g,iC5-nC6}$	$\alpha_{g,HYP1}$	$\alpha_{g,HYP2}$	$\alpha_{g,HYP3}$
Rock type 1														
0.0118	4	1	1	1	1	1	1	4	1	1	1	1	1	1
0.4358	3.456	1.131	1.133	1.137	1.146	1.159	1.198	4	1	1	1	1	1	1
0.8525	5.308	0.826	0.832	0.846	0.879	0.92	0.947	3.96	1.296	1.294	1.287	1.266	1.214	1.199
Rock type 2														
0.0118	4	1	1	1	1	1	1	4	1	1	1	1	1	1
0.0249	1.96	1.015	1.015	1.015	1.016	1.017	1.019	4	1	1	1	1	1	1
0.3675	1.34	1.209	1.211	1.214	1.22	1.228	1.255	4	1	1	1	1	1	1
Rock type 3														
0.0118	4	1	1	1	1	1	1	4	1	1	1	1	1	1
0.3756	4.664	0.888	0.887	0.885	0.879	0.871	0.847	3.992	1.01	1.012	1.014	1.019	1.024	1.058
0.7913	4.384	0.989	0.989	0.99	0.991	0.992	0.993	4	1.023	1.025	1.029	1.045	1.079	1.014
Rock type 4														
0.0118	4	1	1	1	1	1	1	4	1	1	1	1	1	1
0.0919	5.152	0.966	0.966	0.965	0.964	0.962	0.957	4	1	1	1	1	1	1
0.5076	3.888	1.009	1.009	1.01	1.01	1.01	1.009	3.936	1.299	1.29	1.27	1.227	1.189	1.464
Rock type 5														
0.0118	4	1	1	1	1	1	1	4	1	1	1	1	1	1
0.5635	4.396	0.884	0.882	0.878	0.872	0.863	0.828	4.052	0.933	0.932	0.931	0.926	0.918	0.827
0.8079	4.284	0.631	0.728	0.876	1.086	1.233	1.377	4.044	0.821	0.828	0.845	0.889	0.942	0.792
Rock type 6														
0.0118	4	1	1	1	1	1	1	4	1	1	1	1	1	1
0.4904	4.448	0.986	0.985	0.985	0.984	0.983	0.981	4.02	0.954	0.955	0.957	0.959	0.959	0.888
0.8448	4.456	0.91	0.91	0.91	0.913	0.914	0.904	3.996	1.044	1.044	1.043	1.044	1.043	1.084
Rock type 7														
0.0118	4	1	1	1	1	1	1	4	1	1	1	1	1	1
0.3512	3.9	1.005	1.006	1.006	1.006	1.005	1.004	4.032	0.936	0.935	0.929	0.915	0.919	0.92
0.5098	7.22	0.873	0.873	0.872	0.871	0.869	0.857	4.008	0.879	0.882	0.888	0.897	0.905	0.927

Fig. 11 shows the field phase and component production rates. The fraction of CO_2 in the produced gas phase and that of the 4th component ($iC_4 - C_6$) in the produced oil phase for model 2 are shown in Figs. 11(c) and 11(d), respectively. The REs (calculated from Eq. 18) of the coarse-scale models relative to the fine-scale model for Case 2 are presented in Table 7. Like the trends observed in Case 1, the results obtained using the non-calibrated alpha factors and the standard coarse models displayed significant errors in the phase and component production rates. It was also observed that the calibration of the transport coefficients led to the better solutions of the upscaling procedure and errors of less than 6% for all the performance metrics assessed.

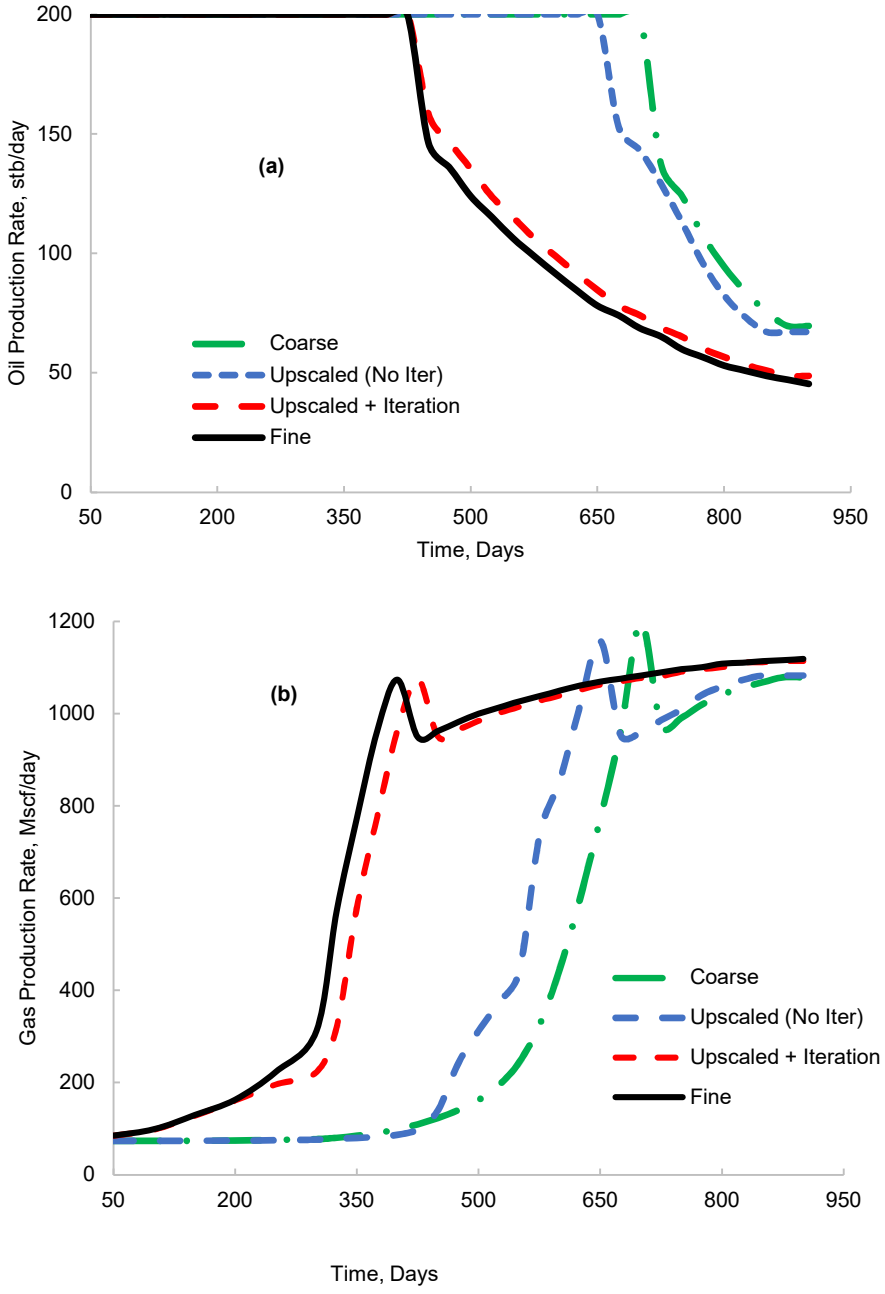

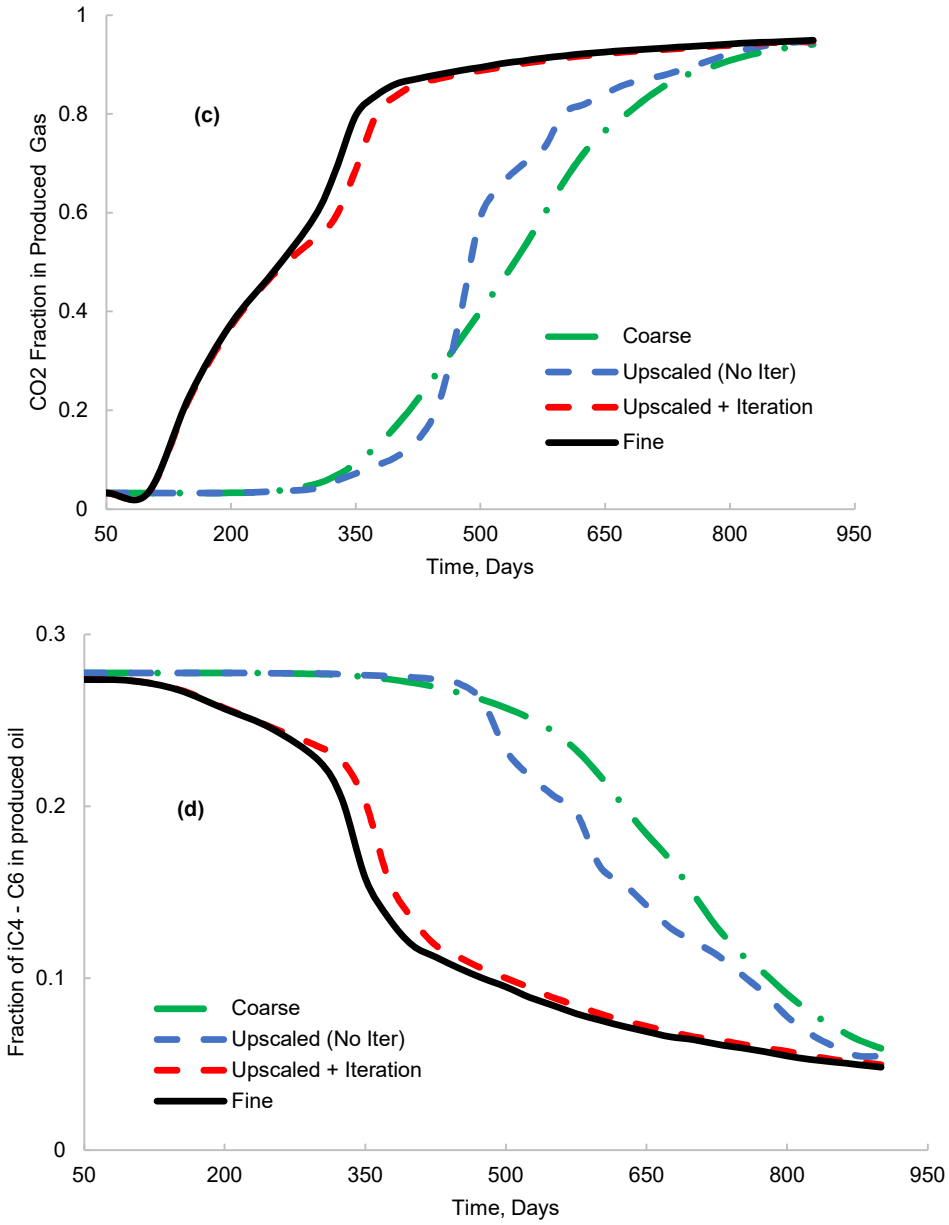

Fig. 11: Fluid production profiles of the fine and the upscaled coarse grid showing (a) oil, and (b) gas production rate. The composition of (c) CO_2 in the produced gas, and (d) the 4th components iC_4 - C_6 in the produced oil phase, of the fine and the upscaled coarse grids are also shown.

Table 7: Summary of the errors of the upscaling results of Model 2.

Simulation Model	Coarse	Upscaled (No Tuning)	Upscaled + Tuning
Oil Production Rate	59.84%	50.65%	4.49%
Gas Production Rate	46.75%	39.93%	5.67%
CO_2 in gas	40.32%	36.9%	1.86%
$iC_4 – C_6$ in oil	96.46%	76.43%	5.47%

We then compared the distribution of CO_2 in the reservoir models as shown in Fig. 12. The fine-scale CO_2 field is shown in Fig. 12a. Fig. 12b shows the results of the CO_2 concentration of the fine-scale grid averaged to the coarse-scale grid using a pore-volume weighted average. The concentration fields for the tuned upscaling, non-calibrated upscaling, and un-upscaled coarse grids are shown in Figs. 12c, 12d, and 12e, respectively. The CO_2 fields from the standard coarse grid and the non-iterated upscaling procedure (Figs. 12d and 12e) clearly overpredicted the distribution of this quantity relative to the fine-scale grids (Fig. 12a) over a vast portion of the model. However, the tuned-upscaling model, seen in Fig. 12c, was in a relatively good agreement with the fine-scale solution relative to the other coarse grids further confirming the capability of this upscaling technique in achieving a better global solution.

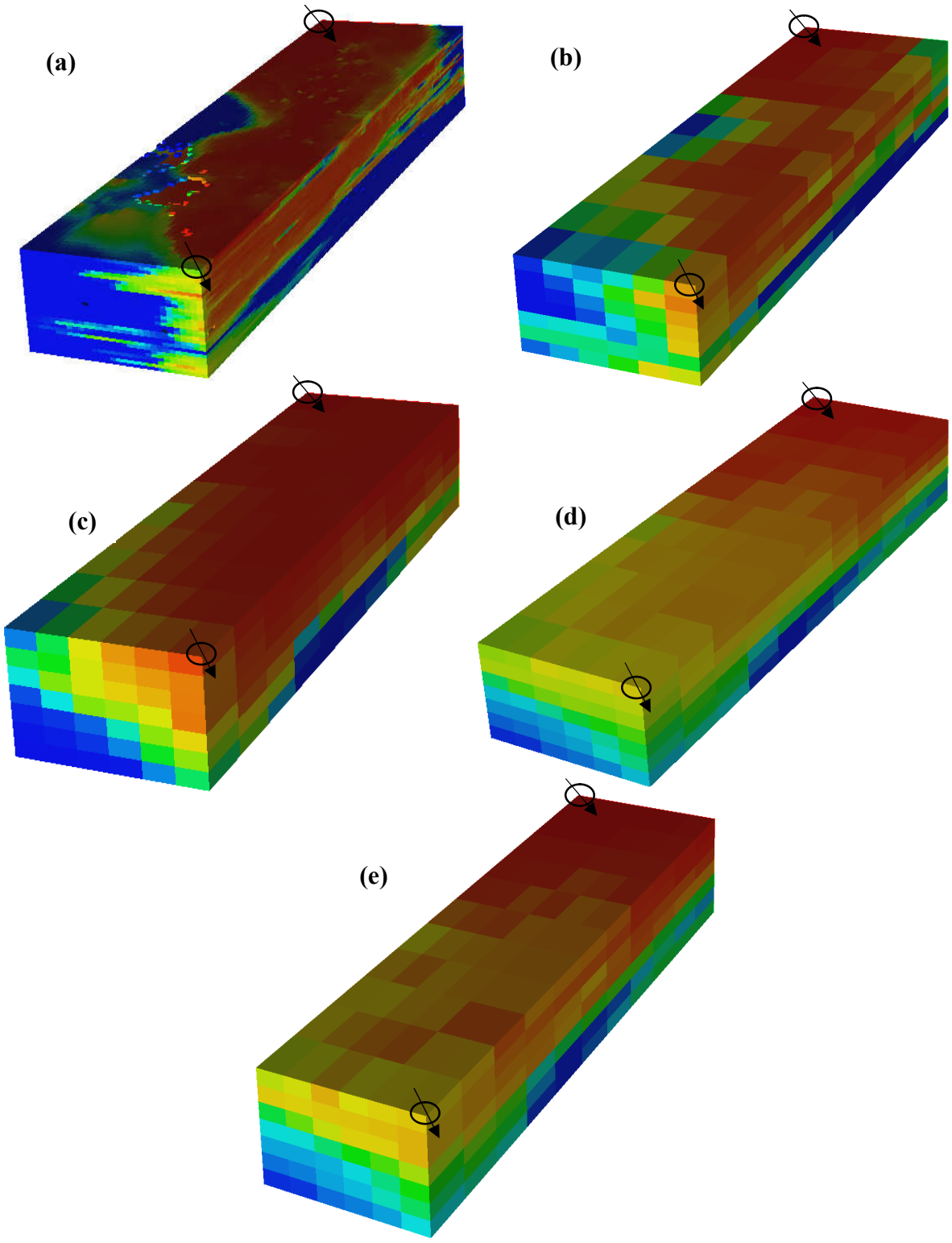

Fig. 12: CO_2 concentration distributions and well locations within the reservoir models at 350 days for (a) fine-scale grid, (b) the pore-averaged fine-scale onto the coarse-scale, (c) iterated alpha factors, (d) non-iterated alpha factors and (e) the standard coarse, models.

Fig. 13 shows the maps of oil saturation in the third layer of the upscaled model. Fig. 13(a) shows the result of the oil saturation of the fine-scale grid averaged to the coarse-scale grid using a pore-volume weighted average. As usual, the predictions using the non-calibrated upscaled grid (Fig. 13(c)) and the standard coarse grid (Fig. 13(d)) were inaccurate. At the same time, the calibrated-upscaling model (Fig. 13(b)) was a closer match to the averaged coarse grid than the other two models.

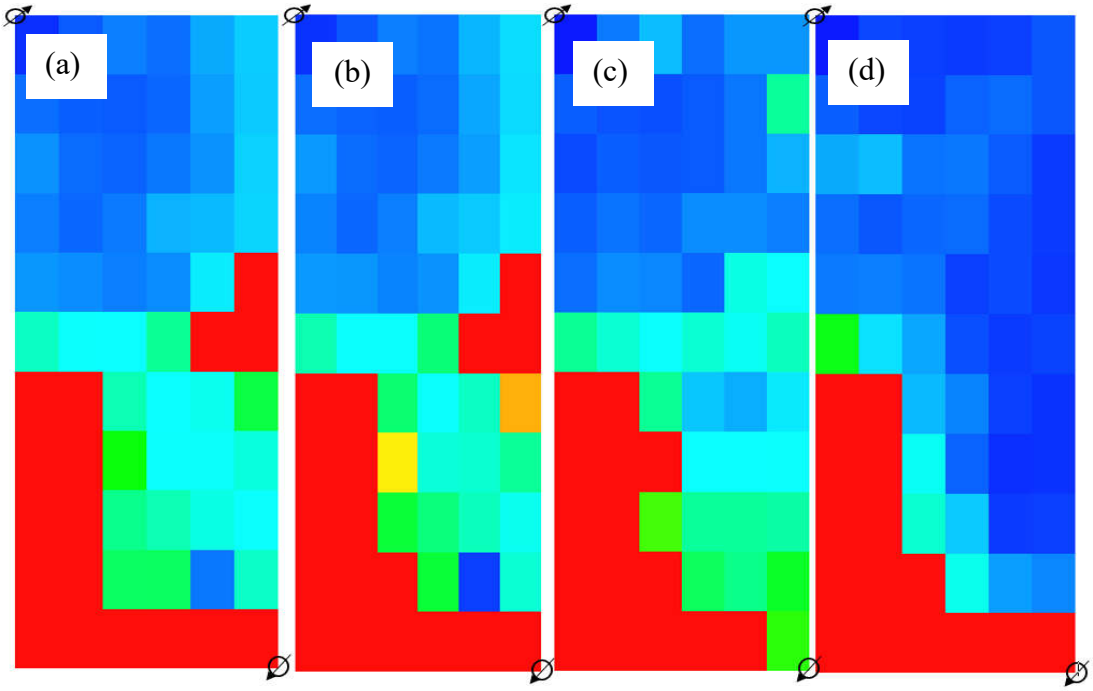

Fig. 13: Oil saturation distributions within the reservoir models in layer 3 at 150 days for (a) the fine grid averaged onto the coarse-scale grid (b) calibrated alpha factors, (c) non-calibrated alpha factors, and (d) standard un-upscaled coarse, models.

The results presented so far involve a constant BHP setting for the injection well and constant oil production rate for the producer. It is therefore necessary to test the reliability of the procedure to other settings. In a field-level optimisation study where we improved the coarse-model accuracy by manually iterating on the alpha factors, we tested the robustness and usability of this upscaling approach to other well control setting (Ogbeiwi, 2023). In this study, the oil production rate and the injector BHP were perturbed by factors of ± 30% and +20%, respectively, from the original settings used in this work. The results obtained displayed a good level of robustness and were relatively accurate over the range of well controls.

Assisted Upscaling using the ANN-based GA optimisation

In the previous section, we present the results of the upscaling procedure. Each full-physics simulation of the coarse-scale model takes 10 minutes to execute, and that this computational cost effects the accuracy of the alpha-factor tuning, it was therefore expedient to seek out a way to improve the efficiency of the transport coefficient calibration process. In this study, we did this by using an ANN-based GA optimisation in an assisted upscaling procedure. In this section, the results of the assisted upscaling are presented.

To limit the number of input variables to those that have a significant influence on the objective function, a sensitivity analysis was performed. The Plackett-Burman design was used to generate the set of simulation runs that were required to assess the effects of the transport coefficients on the initial objective function, i.e., the total RMSE. Each full-physics simulation takes 10 minutes to run as shown in Table 7. The sensitivities of the input variables to the objective function were assessed by varying one variable at a time and their effects were represented as the percentage contribution of each variable to changes in the values of the objective function given as (Arinkoola et al., 2016):

$$\%\ contribution = \frac{|Y_{i,max} - Y_{i,min}|}{\sum|Y_{i,max} - Y_{i,min}|} \times 100\% \qquad (28)$$

Where $Y_{i,max}$ and $Y_{i,min}$ are the maximum and minimum values of the objective function(s) evaluated for the minimum and maximum values of each variable i, respectively. The denominator represents the sum of the numerator for all the variables. The input variables having a % contribution of less than 5% were regarded as insignificant. Based on the results, eight parameters were retained for constructing the proxy model of the final objective function. The Pareto chart of the sensitivity analysis is presented in Fig. 14.

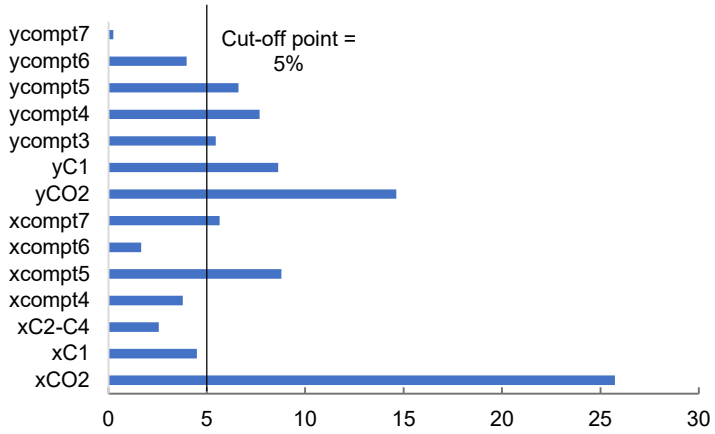

Fig. 14: Summary of the sensitivities of input variable on the objective function.

Thus, the significant input variables are α_{o,CO_2}, $\alpha_{o,C1}$, $\alpha_{o,compt5}$, $\alpha_{o,compt7}$, α_{g,CO_2}, α_{g,C_1},

$\alpha_{g,compt3}$, $\alpha_{g,compt4}$ and $\alpha_{g,compt5}$. The final RMSE was given as:

$$RMSE = f(\alpha_{o,CO_2}, \alpha_{o,C1}, \alpha_{o,compt5}, \alpha_{o,compt7}, \alpha_{g,CO_2}, \alpha_{g,C_1}, \alpha_{g,compt3}, \alpha_{g,compt4}, \alpha_{g,compt5}) \quad (29)$$

and the objective function of the assisted upscaling procedure was:

$$min\{f(\alpha_{o,CO_2}, \alpha_{o,C1}, \alpha_{o,compt5}, \alpha_{o,compt7}, \alpha_{g,CO_2}, \alpha_{g,C_1}, \alpha_{g,compt3}, \alpha_{g,compt4}, \alpha_{g,compt5})\} \quad (30)$$

The GA optimisation was coupled with the surrogate model in MATLAB environment (Mathworks Inc, 2019). Since the computational cost of the numerical simulation of the coarse-scale models is much higher than that of the ANN, using the GA-optimised ANN model in lieu of the full-physics simulation ensured that the upscaling procedure was conducted using fewer simulation runs, and at far lesser computational costs. The computational costs of the fine- and coarse-scale full-physics simulation, each surrogate model evaluation and the optimisation routines using the proxy model in a 3.60 GHz CPU is shown in Table 8.

Table 8: Computational costs of proxy model evaluation and full reservoir simulation

Scenario	CPU cost
Fine-scale full-physics simulation	40 minutes
Coarse-scale full-physics simulation	10 minutes
Proxy model evaluation	10 s
Automatic Tuning using the proxy model	60 s

The optimal results are presented in Table 9. These values are multipliers which were applied to the transport coefficients shown in Table 3, and the RMSE obtained using these values was 0.2799. Fig. 15 shows the plots of the resulting field production rates by the phases, and compositions. It is clearly seen that the assisted-upscaling procedure results in more accurate predictions of the fine-scale model than the manual procedure. Overall, the results showed that the proposed methodology can be applied for the faster upscaling of the fine-scale simulations on coarse-scale models. Applying the proxy model reduced the time required for upscaling to about 60 seconds, although more simulations were required to construct the suitable ANN proxy model, and to assess its accuracy.

Table 9: Optimum values of the transport coefficients.

Variable	$\alpha_{o,C1}$	$\alpha_{o,HYP1}$	$\alpha_{o,HYP3}$	α_{g,CO_2}	$\alpha_{g,C1}$	$\alpha_{g,C2-nC4}$	$\alpha_{g,iC5-nC6}$	$\alpha_{g,HYP1}$	*RMSE*
Value	0.43	0.10	4.40	3.87	0.11	2.02	4.36	0.86	0.2799

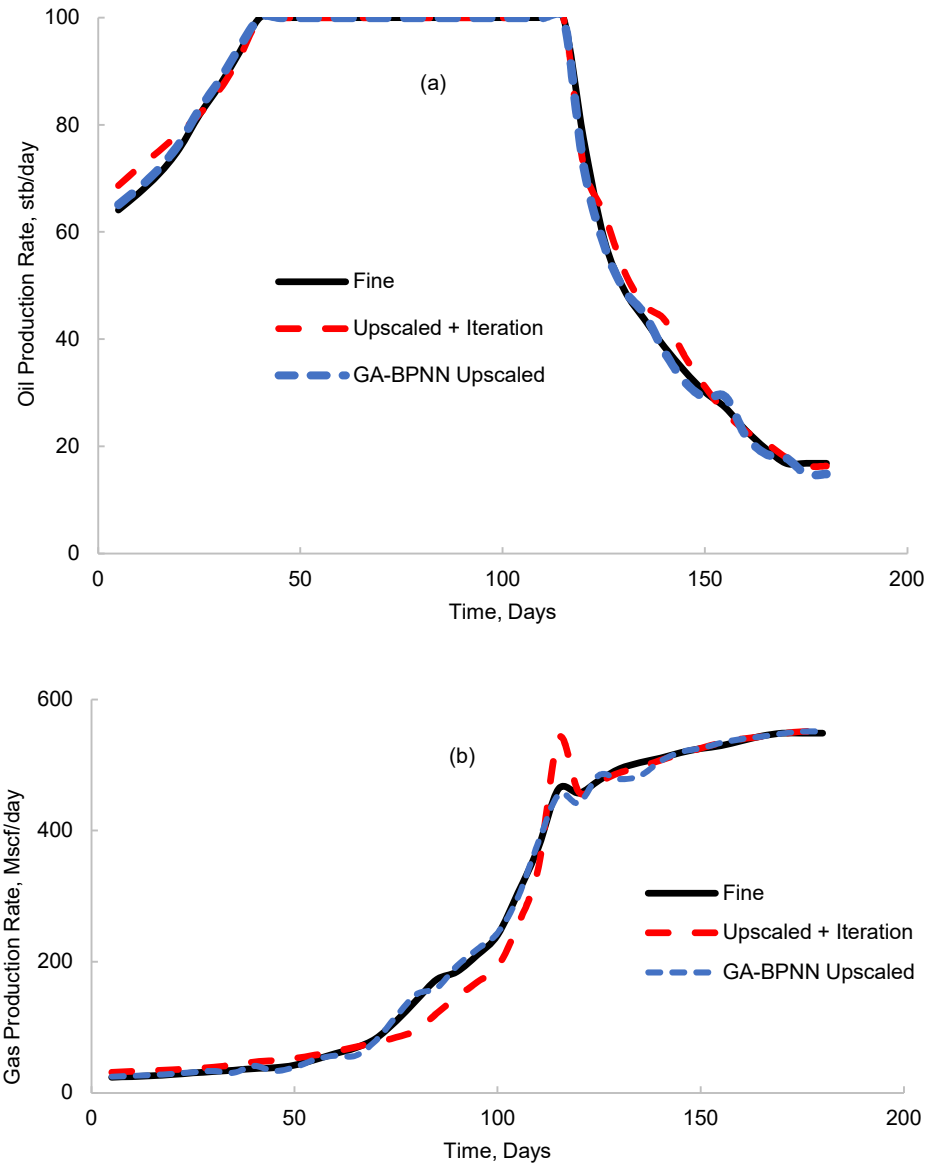

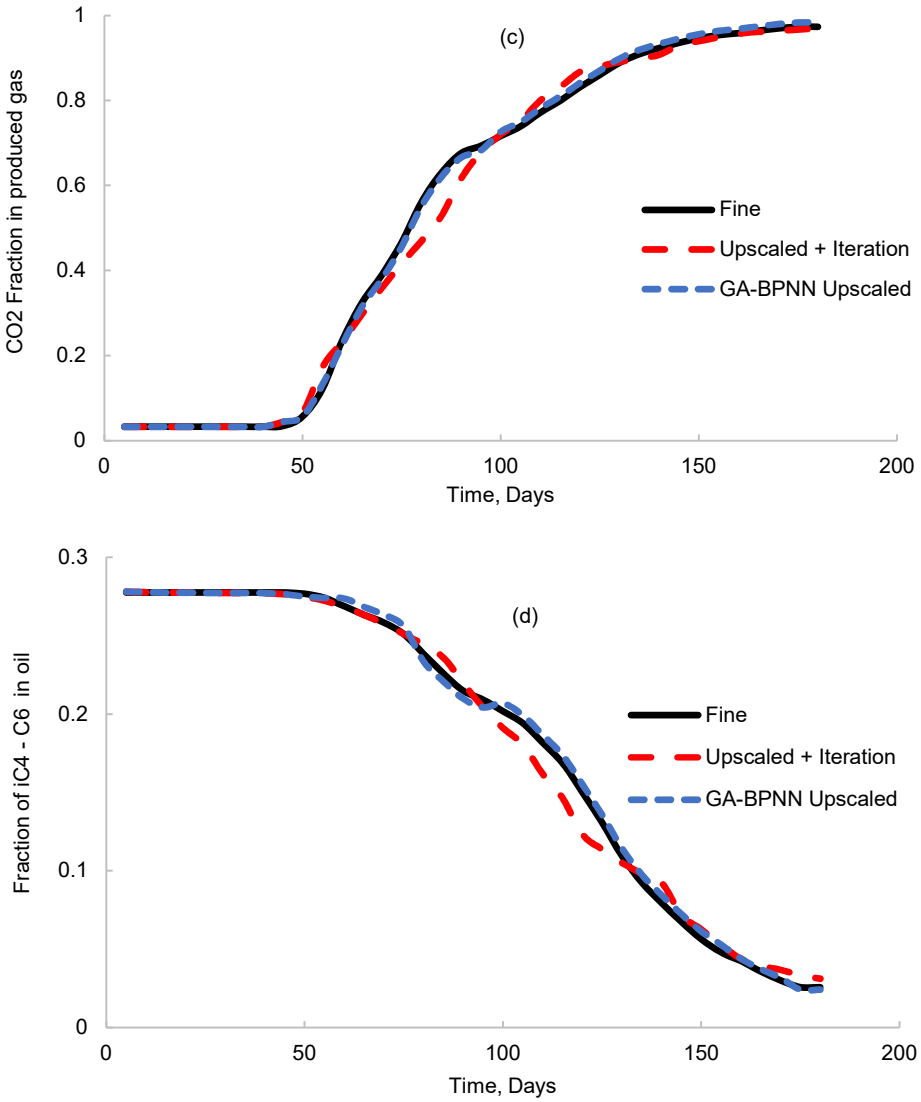

Fig. 15: Fluid production profiles of the fine and the upscaled coarse grid showing (a) oil, and (b) gas production rate. The composition of (c) CO_2 in the produced gas, and (d) the 4th components, iC_4 - C_6 in the produced oil phase, of the fine and the upscaled coarse grids are also shown.

In order to validate the results obtained from the assisted upscaling procedure, a final confirmation test was conducted by applying the predicted optimal variables to a full-physics simulation, and then computing the RMSE. This resulted in an RMSE of 0.276, representing a relative percentage error of 1.5% which showed that the simulation result was in good agreement with the proxy predicted value.

Overall, the results of the GA-BPNN assisted calibration of the transport coefficients showed that the proposed methodology can be applied for the faster upscaling of the fine-scale simulations on coarse-scale models. Applying the proxy model reduced the time required for

upscaling to about 60 seconds, although more simulations were required to construct the suitable ANN proxy model, and to assess its accuracy.

Summary and Conclusions

The use of fine-scale compositional simulations to model miscible CO_2 flooding is highly computationally expensive, and upscaling procedures can be used to approximate the behaviour of these fine-scale grids on more realistic coarse-scale models. During upscaling, a mismatch between the phase fluxes of the integrated fine-scale and that of the coarse-scale is observed. This can be reduced improved by tuning some of the derived upscaled coarse-scale quantities like is done in reservoir history matching problems. However, this process is generally also computationally expensive and subject to human errors.

This study presents a framework to reduce the computational expense associated with compositional upscaling. We proposed a novel methodology for upscaling miscible floods using a neural-network-based genetic-algorithm-assisted upscaling procedure. We also represented the dynamics of small-scale molecular diffusion, and macro-scale heterogeneity-induced channelling associated with miscible CO_2 displacements on the upscaled coarser grid reservoir models based on the pseudoisation of relative permeability and transport coefficients. This framework adequately represented small- and field- scale physical instabilities such as molecular diffusion and heterogeneity-induced fingering on coarser grids. Based on the results obtained, the following conclusion were reached:

1. The pseudoisation of relative permeabilities which ensures the matching of large-scale effects such as the volumetric fluxes of the phases and the use of transport coefficients to better represent small-scale interactions such as the time-dependent flux of the components within the hydrocarbon phases (molecular diffusion)
2. While the use of pseudo relative permeabilities alone may guarantee matching the volumetric flow of the phases alone, the use of alpha factors in upscaling compositional models led to better representations of small-scale physical effects. According to our results, when this is done efficiently, the pseudoisation of the relative permeability pseudo-functions can be neglected, and the accuracy of the upscaling procedure depends on the accuracy of the upscaled transport coefficients.
3. The assisted calibration of the alpha factors offers an efficient approach to the upscaling of compositional fluid flow. When combined with a data-driven

approximation model, the associated computational expense associated tuning can be significantly reduced.

Nomenclature

α = alpha

p = phase

F_i = molar flux of component i

ρ_o= density of oil

ρ_g= density of oil

x_i= mole fraction of the liquid phase

y_i= mole fraction of the gas phase

U_o= oil phase flow velocity

U_g = gas phase flow velocity

q_t= total fluid flow velocity

V_p= pore volume

S_p= saturation of phase, p

f_p= fractional flow of the phase, p

T= transmissibility

λ= mobility

μ_p = viscosity of phase p

K = permeability

z_{CO_2}= mole fraction of CO_2

NN = neural network

GA = genetic algorithm

Acknowledgements

The authors wish to acknowledge the Petroleum Technology Development Fund (PTDF) for supporting this study. Schlumberger is also acknowledged for the provision of the ECLIPSE 300 simulator used in this study.

References

Agada, S., Geiger, S., Elsheikh, A., Oladyshkin, S., 2017. Data-driven surrogates for rapid simulation and optimization of WAG injection in fractured carbonate reservoirs. Pet.

Geosci. 23, 270–283. https://doi.org/10.1144/petgeo2016-068

Aghbash, V.N., Ahmadi, M., 2012. SPE 153920 Evaluation of CO2-EOR and Sequestration in Alaska West Sak Reservoir Using Four-Phase Simulation Model. Spe 153920 16. https://doi.org/10.2118/153920-MS

Aghdam, K.A., Ghorashi, S.S., 2017. Critical Parameters Affecting Water Alternating Gas (WAG) Injection in an Iranian Fractured Reservoir 7, 3–14.

Ajose, D., Mohanty, K.K., 2003. Compositional Upscaling in Heterogeneous Reservoirs: Effect of Gravity, Capillary Pressure, and Dispersion. Proc. - SPE Annu. Tech. Conf. Exhib. 2661–2668. https://doi.org/10.2523/84363-ms

Akinyele, O., Stephen, K., 2020. Numerical effects of fluid flow modelling in surfactant chemical flooding. ECMOR 2020 - 17th Eur. Conf. Math. Oil Recover. https://doi.org/10.3997/2214-4609.202035135

Alireza, K., D, S.K., 2012. Schemes for automatic history matching of reservoir modeling : A case of Nelson oilfield in UK. Pet. Explor. Dev. 39, 349–361. https://doi.org/10.1016/S1876-3804(12)60051-2

Arinkoola, A.O., Onuh, H.M., Ogbe, D.O., 2016. Quantifying uncertainty in infill well placement using numerical simulation and experimental design: case study. J. Pet. Explor. Prod. Technol. 6, 201–215. https://doi.org/10.1007/s13202-015-0180-z

Barker, J.W., Fayers, F.J., 1994. Transport coefficients for compositional simulation with coarse grids in heterogeneous media. SPE Adv. Technol. Ser. 2, 103–112. https://doi.org/10.2118/22591-pa

Barker, J.W., Prévost, M., Pitrat, E., 2005. Simulating residual oil saturation in miscible gas flooding using alpha-factors. SPE Reserv. Simul. Symp. Proc. 423–430. https://doi.org/10.2523/93333-ms

Barker, J.W., Thibeau, S., 1997. A Critical Review of the Use of Pseudorelative Permeabilities for Upscaling. SPE Reserv. Eng. 12, 138–143. https://doi.org/10.2118/35491-PA

Blunt, M., Fayers, F.J., Orr, F.M., 1993. Carbon dioxide in enhanced oil recovery. Energy Convers. Manag. https://doi.org/10.1016/0196-8904(93)90069-M

Camy, J.P., Emanuel, A.S., 1977. Effect Of Grid Size In The Compositional Simulation Of CO2 Injection. SPE Annu. Fall Tech. Conf. Exhib. https://doi.org/10.2118/6894-MS

Chang, Y.-B., Lim, M.T., Pope, G.A., Sepehrnoori, K., 1994. CO2 flow patterns under multiphase flow: heterogeneous field-scale conditions. SPE Reserv. Eng. (Society Pet. Eng. 9, 208 – 216. https://doi.org/10.2118/22654-pa

Chen, Y., Mallison, B., Durlofsky, L., 2008. Nonlinear two-point flux approximation for modeling full-tensor effects in subsurface flow simulations. Comput. Geosci. 12, 317–335. https://doi.org/10.1007/s10596-007-9067-5

Christie, M.A., Blunt, M.J., 2001. Tenth SPE comparative solution project: A comparison of upscaling techniques. SPE Reserv. Eval. Eng. 4, 308–316. https://doi.org/10.2118/72469-pa

Christie, M.A., Clifford, P.J., 1998. Fast Procedure for Upscaling Compositional Simulation. SPE J. 3, 272–278. https://doi.org/10.2118/50992-PA

Costa, L.A.N., Maschio, C., José Schiozer, D., 2014. Application of artificial neural networks in a history matching process. J. Pet. Sci. Eng. 123, 30–45. https://doi.org/10.1016/j.petrol.2014.06.004

Dai, Z., Viswanathan, H., Xiao, T., Middleton, R., Pan, F., Ampomah, W., Yang, C., Zhou, Y., Jia, W., Lee, S.Y., Cather, M., Balch, R., McPherson, B., 2017. CO2Sequestration and Enhanced Oil Recovery at Depleted Oil/Gas Reservoirs. Energy Procedia 114, 6957–6967. https://doi.org/10.1016/j.egypro.2017.08.034

Dang, C.T., Nghiem, L.X., Nguyen, N.T., Chen, Z., Yang, C., 2016. Integrated Modeling for Assisted History Matching and Production Forecasting of Low Salinity Waterflooding. https://doi.org/10.3997/2214-4609.201600766

Darman, N.H., Pickup, G.E., Sorbie, K.S., 2002. A comparison of two-phase dynamic upscaling methods based on fluid potentials. Comput. Geosci. 6, 5–27. https://doi.org/10.1023/A:1016572911992

Fayers, F.J., Barker, J.W., Newley, T.M.J., 1989. Effects of Heterogeneities on Phase Behaviour in Enhanced Oil Recovery.

Fayers, F.J., Haajizadeh, M., Lin, C.Y., Taggart, J., 2007. Use of the 4-Component Todd and Longstaff Method as an Upscaling Technique in Simulating Gas Injection Projects 1–15. https://doi.org/10.2523/59340-ms

Foroud, T., Seifi, A., AminShahidi, B., 2014. Assisted history matching using artificial neural network based global optimization method - Applications to Brugge field and a fractured Iranian reservoir. J. Pet. Sci. Eng. 123, 46–61. https://doi.org/10.1016/j.petrol.2014.07.034

Garmeh, G., Johns, R.T., 2010. Upscaling of miscible floods in heterogeneous reservoirs considering reservoir mixing. SPE Reserv. Eval. Eng. 13, 747–763. https://doi.org/10.2118/124000-pa

Jákupsstovu, S., Zhou, D., Kamath, J., Durlofsky, L., Stenby, E.H., 2001. Upscaling of

Miscible Displacement Processes. 6th Nord. Symp. Petrophysics, May 15-16 15–16.

Jerauld, G.., 1998. A Case Study in Scaleup for Multi-contact Miscible Hydrocarbon Gas Injection. SPE Reserv. Eval. Eng. 1, 575–582.

Karimaie, H., Nazarian, B., Aurdal, T., Nøkleby, P.H., Hansen, O., 2017. Simulation Study of CO2EOR and Storage Potential in a North Sea Reservoir. Energy Procedia 114, 7018–7032. https://doi.org/10.1016/j.egypro.2017.03.1843

Kyte, J.R., Berry, D.W., 1975. New Pseudo Functions To Control Numerical Dispersion. Soc Pet Eng AIME J 15, 269–276. https://doi.org/10.2118/5105-pa

Li, H., Durlofsky, L.J., 2016a. Upscaling for compositional reservoir simulation. SPE J. 21, 873–887. https://doi.org/10.2118/173212-pa

Li, H., Durlofsky, L.J., 2016b. Ensemble level upscaling for compositional flow simulation. Comput. Geosci. 20, 525–540. https://doi.org/10.1007/s10596-015-9503-x

Luo, H., Delshad, M., Pope, G.A., Mohanty, K.K., 2018. Scaling up the interplay of fingering and channeling for unstable water/polymer floods in viscous-oil reservoirs. J. Pet. Sci. Eng. 165, 332–346. https://doi.org/10.1016/j.petrol.2018.02.035

Mathworks Inc, 2019. MATLAB.

Minton, J.J., 2012. S01251[1] 122–141.

Negash, B.M., Vel, A., Elraies, K.A., 2017. Artificial neural network and inverse solution method for assisted history matching of a reservoir model. Int. J. Appl. Eng. Res. 12, 2952–2962.

Ogbeiwi, P., 2023. WATER-ALTERNATING-GAS ENHANCED OIL RECOVERY OPTIMISATION FOR GREATER CO2 STORAGE AND OIL RECOVERY IN A MATURE TURBIDITE RESERVOIR: CASE STUDY OF THE NIGER DELTA. Heriot-Watt University.

Ogbeiwi, P, Stephen, K., Arinkoola, A., 2020. A Surrogate-Based Approach to Waterflood Optimisation under Uncertainty 2020, 1–16. https://doi.org/https://doi.org/10.3997/2214-4609.202035076

Ogbeiwi, Precious, Stephen, K.D., Arinkoola, A.O., 2020. Robust optimisation of water flooding using an experimental design-based surrogate model: A case study of a Niger-Delta oil reservoir. J. Pet. Sci. Eng. 195, 107824. https://doi.org/10.1016/j.petrol.2020.107824

Orr, F.M., 2004. Storage of Carbon Dioxide in Geologic Formations. J. Pet. Technol. 56, 90–97. https://doi.org/10.2118/88842-JPT

Rios, V.S., Santos, L.O.S., Quadros, F.B., Schiozer, D.J., 2019. New upscaling technique for

compositional reservoir simulations of miscible gas injection. J. Pet. Sci. Eng. 175, 389–406. https://doi.org/10.1016/j.petrol.2018.12.061

Stone, H.L., 1991. Rigorous black oil pseudo functions. Proc. SPE Symp. Reserv. Simul. 57–68. https://doi.org/10.2523/21207-ms

Thibeau, S., Barker, J.W., Souillard, P., 1995. Dynamical Upscaling Techniques Applied to Compositional Flows 363–373. https://doi.org/10.2118/29128-ms

Zhang, H.R., Sorbie, K.S., 1995. Upscaling of miscible and immiscible displacement processes in porous media. Proc. Int. Meet. Pet. Eng. 1, 427–440.

Zhang, X.S., Hou, J., Wang, D.G., Mu, T.H., Wu, J.T., Lu, X.J., 2012. An automatic history matching method of reservoir numerical simulation based on improved genetic algorithm. Procedia Eng. 29, 3924–3928. https://doi.org/10.1016/j.proeng.2012.01.595